



Shear behaviour of the post-tensioned segmental precast concrete pontoon deck with the GFRP rods

Shahrad Ebrahimzadeh^a, Allan Manalo^a, Omar Alajarmeh^{a,*}, Charles Dean Sorbello^b,
Senarath Weerakoon^b, Reza Hassanli^c, Brahim Benmokrane^d

^a Centre for Future Materials (CFM), Institute for Advanced Engineering and Space Sciences (IAESS), University of Southern Queensland, Toowoomba 4350, Australia

^b Maritime Safety Queensland, Department of Transport and Main Roads, Brisbane, Qld 4000, Australia

^c UniSA STEM, University of South Australia, Mawson Lakes, SA 5095, Australia

^d University of Sherbrooke, Department of Civil & Building Engineering, Sherbrooke, Quebec J1K 2R1, Canada

ARTICLE INFO

Keywords:

Post-tensioned segmental deck
Precast concrete
GFRP
Numerical modelling
Shear strength

ABSTRACT

The present experimental and numerical study evaluated the structural performance of segmental concrete pontoon decks reinforced and post-tensioned with GFRP rods. Four large-scale decks were tested and the load-displacement response, strain behaviour of rods, concrete, and failure mechanism in four different prestressing levels were assessed. It was found that a small post-tensioning of 7.4 % of the rod's ultimate tensile strength reduced the self-weight deflection by 92 % and increased initial stiffness by 8.7 times compared to segmental decks without prestressing. Failure in prestressing decks typically began with concrete crushing at the joint with an increased compression depth due to increased initial post-tension; however, the ultimate failure mechanism of the hand-tight deck was governed by the interlaminar shear of the rod. A finite element model was developed and verified against test results. A parametric study evaluating the influence of the post-tensioning at higher load, rod depth, concrete properties, rod number, and deck geometry was implemented. It was shown that increasing the post-tension load and depth of the rod improved the stiffness and reducing the spacing can result in a more uniform compression stress in the joint. This study provides design recommendations for ACI 440.4 R-04, by considering the concrete compression depth between joints rather than the depth of the FRP rod and contributes to a more accurate load estimation of the concrete crushing caused by joint openings. The results of this research could rectify the present problems with the construction design of maritime infrastructure and offer an innovative solution.

1. Introduction

The corrosion of steel rebars is causing significant degradation of reinforced concrete structures, creating an economic burden and leading to catastrophic incidents. A renowned case is the Ynys-y-Gwas Bridge which failed because of the penetration of salt water into the joint, which leads to corrosion and eventually tendon rupture [1]. No fatalities were recorded, but this incident demonstrated that the failure of the structure because of steel corrosion can happen without any notice. The corrosion problem in concrete structures may also affect over AU\$ 1.1 trillion worth of homes, commercial buildings, ports, and other physical infrastructure assets built in or near the coastal regions of Australia [2]. This accounts for almost 70 % of the Australian GDP in 2020 [3]. This significant problem of steel corrosion has increased interest in using

glass fibre-reinforced polymer (GFRP) bars as an efficient and non-corrosion alternative for the internal reinforcement of concrete structures.

GFRP bars have excellent durability against aggressive environmental conditions including high alkaline environment [4–6], chloride exposure [7,8], wet-dry and freeze-thaw cycles [9], extreme temperature variations [10], seawater exposure [11–14], ultraviolet radiation [15], and elevated in-service temperatures [16]. Numerous studies have also demonstrated the excellent structural performance of GFRP-reinforced concrete marine structures, including pontoon decks [17,18], piles [19,20], water tanks [21], docks [22,23], jetties [24], girder [25], and boat ramps [26], establishing it as a reliable, economical, and practical internal reinforcement to concrete structures.

Prefabricated concrete construction reinforced with GFRP bars improves efficiency by enabling the manufacturing and assembly of

* Corresponding author.

E-mail address: omar.alajarmeh@unisa.edu.au (O. Alajarmeh).

<https://doi.org/10.1016/j.istruc.2024.107798>

Received 29 August 2024; Received in revised form 28 October 2024; Accepted 6 November 2024

Available online 14 November 2024

2352-0124/© 2024 The Author(s). Published by Elsevier Ltd on behalf of Institution of Structural Engineers. This is an open access article under the CC BY license (<http://creativecommons.org/licenses/by/4.0/>).

Nomenclature

A_f	Area of the FRP reinforcement.
A_k	The area of the shear key in the joint in the failure plan.
A_{sm}	The area of contact between the smooth surface on the failure plan.
b	Deck's width.
b_w	Minimum effective web width.
d	Distance from the extreme compression fibre to the centroid of longitudinal tension force.
E_f	Modulus of elasticity of GFRP.
f_c	Compressive strength of concrete.
f_f	GFRP rod's stress.
f_{fe}	Effective prestressing stress.
k	Ratio depth of neutral axis to reinforcement depth.
V_c	Shear resistance.
ϵ_{cu}	Ultimate concrete strain at the extreme compression fibre.
ρ_f	Reinforcement ratio.
ρ_{fb}	Balanced reinforcement ratio.
λ	factor to account for concrete density.
σ_n	Normal compressive stress in concrete.
ψ	Dilation angle.

structures in a shorter time frame [27]. Prefabrication reduces the likelihood of environmental disturbances associated with on-site concrete pouring during construction. However, the low elasticity modulus of GFRP can negatively affect the prefabricated concrete system by large stress concentration on the joint. Therefore, prefabricated concrete members need to be prestressed to tie together, and using a GFRP internal rod addresses concerns about system durability by preventing the penetration of environmental factors into the joint. Furthermore, prestressed rod offers repair capability after major incidents [27,28]. This advantage becomes important as some pontoon decks during the 2022 Queensland flood suffered from local failure close to the joint (Fig. 1). Extensive research has investigated the structural performance of prestressed or post-tensioned segmental concrete beams, slabs, or decks using internal or external steel reinforcement [29–31], and recent studies [32–34] have focused into the flexural response of segmental members post-tensioned by FRP tendons. However, the behaviour of the joint and rod in the precast segmental concrete members is critical as



Fig. 1. Localised damage near the joint on the pontoon decks during the 2022 Queensland and New South Wales flood.

previous studies have shown that in various types of precast concrete members, high-stress concentrations near the joint govern the failure mechanism and lead to premature failure of the beam [35]. This issue can be exacerbated when the load is directly applied to the joint, indicating the need for adjustments to distribute stress more uniformly. Such adjustments require thorough investigation, as El-Naqeeb et al. [27] noted that prestressing through the bolt, combined with epoxy injection, might cause micro-cracking or debonding in the duct, affecting load transfer. In the case of hand-tight concrete joints, increasing the longitudinal reinforcement ratio of GFRP connectors can enhance strength and stiffness [27,36]. Additionally, providing confinement reinforcement can limit crack development around the joint and prevent premature failure [37]. The interconnection between blocks and compressing segments together can positively influence the shear behaviour of the joint [38]. These studies showed the possibility of direct loading onto the joint during the service life of the segmental concrete system, leading to shear loading on the internal rod which indicates the joint behaviour in this system needs to be investigated.

The concept and benefits of the segmental pontoon deck, post-tensioned with GFRP rods were introduced by Ebrahimzadeh et al. [39] and this study evaluated the response of the segmental deck when the applied load is directly above the joint. An experimental program was conducted and a numerical model for hand-tightened and post-tensioned decks was developed and calibrated against the experimental results. A parametric study was then performed to comprehensively examine the influence of loading point, concrete properties, post-tensioning at a higher level, interlock, rod's number, rod's depth, internal reinforcement, deck's geometry, and mesh size in modelling. Accordingly, a design recommendation throughout an analytical evaluation was proposed to reliably predict the shear strength of the segmental concrete deck post-tensioned by internal GFRP rods. The study's outcome can address the current in the maritime infrastructure's construction design and provide a novel solution by using a non-corrosive GFRP-reinforced concrete member.

2. Experimental program

2.1. Design criteria

The concrete segment was designed and manufactured following the guidelines outlined by the Queensland Department of Transport and Main Roads DTMR-2019 [40] for precast concrete members. This guideline specifically targets prefabricated concrete segments having a design life that surpasses 50 years. The segmental concrete pontoon deck samples were designed based on the specifications for floating walkways and pontoon infrastructure in the Queensland DTMR-2015 [41] and New South Wales (NSW Boat Ramp Facility Guidelines [42]) guidelines.

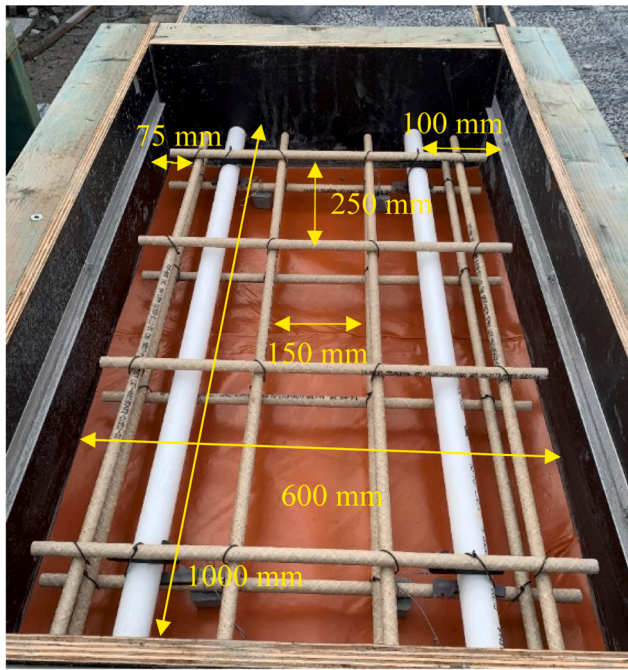
2.2. Material characteristics

2.2.1. Concrete

The concrete used for the testing adhered to the technical specification of MRTS 70 used in Queensland Transport and Main Road, which applies to the construction of concrete, and bridge structures, and may apply to other concrete elements DTMR-2018 [43]. This guideline aligns with AS3600 [44] for the exposure classification C2 (near seawater). Twelve cylindrical specimens were tested following AS1012.9 [45] standards to assess the concrete's compressive strength (f_c) with a mean value of 37.1 MPa and a standard deviation of 6.2 MPa. Although the final average compressive strength is lower than the exposure classification of C2; however, using a non-corrosive GFRP rebar and rod makes the segments suitable for use in marine environments.

2.2.2. Reinforcement anchorage system

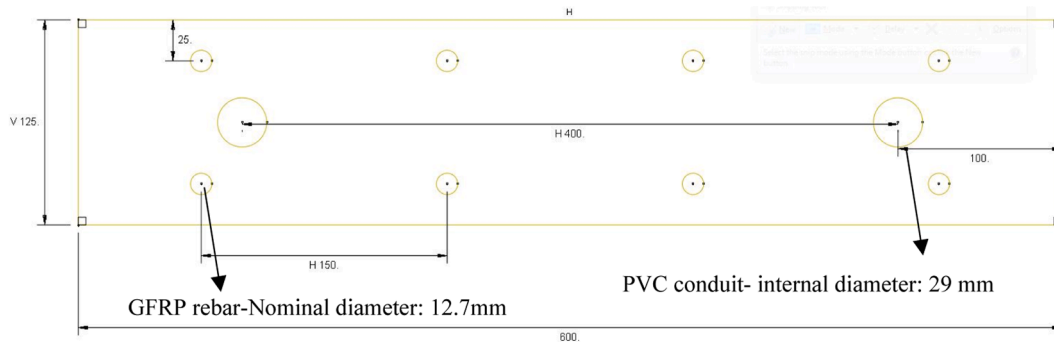
Each deck sample was internally reinforced with Grade III (#4) GFRP bars (Fig. 2a) with a nominal diameter of 12.7 mm, which met the



(a) Internal reinforcement



(b) End anchorage



(c) Cross-sectional diagram details

Fig. 2. Reinforcing details and test set-up for segmental deck.

manufacturing criteria specified in CSA S807 [46] and ASTM D7205 [47]. The engineering characteristics and more details of the internal bars were reported by AlAjarmeh et al. [48]. The threaded GFRP bars denoted as rods in this study and detailed in Table 1, adopted from [39],

Table 1
Rod and anchor properties (Ebrahinzadeh et al., 2024a) [39].

GFRP rods		
Property	Test method	Value
Nominal diameter (mm)	CSA S806 –19	23.5
Cross-sectional area (mm ²)	CSA S806 –19	416
Tensile strength (MPa)	CSA S806 –19	1340
Modulus of Elasticity (GPa)	CSA S806 –19	65
Ultimate strain (%)	CSA S806 –19	2
Fiber content (%)	ASTM D2584 –18	81.9
End anchorage		
Property	Value	Standard deviation
Maximum tensile load (kN)	328.1	9.4
Tensile strength (MPa)	756.8	21.6
Ultimate strain (%)	0.86	0.07

were manufactured following CSA S807 [46].

A threaded stainless-steel tube with a length of 150 mm, an inner diameter of 25 mm, and an outer diameter of 37 mm was employed at both ends of the rod (Fig. 2b) to apply the post-tension. A 38 mm inner diameter steel nut was used for segment connection and post-tensioning force application. A 100 mm × 100 mm square steel plate with a thickness of 20 mm was placed between the steel tube and the concrete surface to minimise stress concentration (Fig. 2). After passing the rod through the segments, the steel nuts were tightened with a wrench and specimens were pre-tensioned. This system provides an easy and practical way to apply a pre-tension load on the construction site without the need for expert labours. The pre-tensioning load was determined by the maximum strength between the GFRP rod and the tube in the anchorage, which was below the limit provided in ACI 440.4 R-04 [49], with pre-stressing limited to 40 % of the maximum tendon’s tensile strength. The recommended limit is proposed to avoid the creep failure of the FRP tendon/rod. More detailed information on the material characteristics can be found in [39].

2.3. Specimens detail

Four large-scale specimens, each comprising two concrete segments, with dimensions of 1000 mm × 600 mm × 125 mm (length × width × thickness), were assembled and tested. The width and thickness adhered to dimensional specifications outlined in DTMR-2015 [41], accounting for the pontoon's floating and structural components. The segment's length was determined by dividing the typical modular length of the pontoon, which varies in different projects. The thickness the deck is based on a full-scale deck for a floating pontoon. A representative width of 600 mm is however taken understand the shear behaviour of the GFRP reinforced deck.

The nomenclature for the deck specimens indicates the post-tension load on each rod, measured by the load cell during the pre-tensioning (Table 2). The transverse and longitudinal spacings of 250 mm and 150 mm (Fig. 2a) led to a transverse and longitudinal reinforcement ratio ($\rho_f = \frac{A_f}{bd}$) of 1.01 % and 1.68 % per segment, respectively. Further details of the section, i.e., rebar spacing, concrete cover, etc are demonstrated in Fig. 2c.

The balanced reinforcement ratio of the prestressed concrete beam, followed by ACI 440.4 R-04 [49], can be obtained using (Eq. 1). For the segmental deck, this results in a different value (depending on the level of pre-stressing) in the range of 0.15 % to 0.24 %, where ϵ_{fe} is the strain in the FRP rod caused by the initial prestressing.

$$\rho_{fb} = 0.85\beta_1 \frac{f_c}{f_{fu}} \times \frac{\epsilon_{cu}}{\epsilon_{cu} + \epsilon_{fu} - \epsilon_{fe}} \quad (1)$$

Also, the maximum compressive strain of the concrete, ϵ_{cu} , is taken as 0.003 following the ACI 440.1 R-15 [50]. Considering the GFRP rod contributing as a reinforcement, the segmental deck's reinforcement ratio (ρ_f) equals 2.22 %.

2.4. Instrumentation and setup

The segmental decks were subjected to 3-point static loading and the 2000 kN Enerpac hydraulic jack applied the load through a spreader steel I-beam with a flange width of 300 mm situated just next to the joint minimizing concrete crushing as the joint opens and achieving the highest shear force (Fig. 3). Due to some limitations in the test feasibility and loadcell measurement, the exposure of the joint to direct load was not possible; however, this simulates the situation when the load is subjected to the joint. The applied load was measured using a 2000 kN load cell. Two load cells were positioned between the steel nut and steel plate to measure the initial post-tension load and the load increment in the rod during the test (Fig. 2b). The applied load, prestressing load on the rods, and strains were recorded using a data acquisition system. Strain in the rod was measured using 3 mm-long electrical-resistance strain gauges, positioned at mid-span, in the vicinity of the joint. Also, a strain gauge was attached to the internal GFRP reinforcement to measure tensile and compression strains. A digital image correlation was utilized to capture the deflection along the length of the deck including the mid-span deflection.

Table 2
Level of post-tensioning force applied to the segmental decks.

Specimen	Post-tensioning force (kN)	Equivalent stress (MPa)	Rod's tensile strength (%)	Anchor's capacity (%)
S0-EXP	Hand tight (< 2.5 kN)	0.6	0.04	0.08
S21-EXP	21.6	49.8	3.7	6.6
S32-EXP	32.1	74.1	5.5	9.8
S42-EXP	42.9	99.1	7.4	13.1

3. Experimental result and discussion

The effect of the initial post-tensioning on the load-carrying capacity, rod's axial load increment-deflection, load-strain, and failure behaviour has been investigated throughout the experimental program.

3.1. Load-carrying capacity-deflection behaviour

The measured deflection resulting from the self-weight of the hand-tight deck (S0-EXP) was 37.2 mm. Upon the application of the pre-tension load of 42 kN on each rod, or compressive stress of 1.14 MPa on concrete, this deflection decreased to 2.9 mm a reduction of 92.2 % (Fig. 4). This reduction is attributed to the increased friction between the segments because of the applied post-tension force, which provides greater resistance against gravity, as it previously observed by in segmental concrete deck with CFRP tendon [32–34] and GFRP rods [39].

The increase in the rod's pre-tension load improved the initial stiffness of the system (Fig. 5a). The improvement in stiffness led to an increase in the load corresponding to the joint opening. This enhancement is attributed to the increase in the neutral axis depth (compression depth between the segments) resulting from the heightened initial post-tension (Table 3). This deduction is drawn from the section analysis when the joint remains closed at the bottom, and the top part of the concrete initiates crushing, allowing beam theory relations in segmental beams to remain. The neutral axis depth was calculated with (Eq. 2) achieved from the section equilibrium equation, as it previously indicated by [39].

$$c = \frac{2A_f(f_f + f_{fe})}{0.85f_c b \beta_1} \quad (2)$$

β_1 calculated from the equation in (ACI 440.1 R-15) [50] and is equal to 0.78, b is equal to the width of the deck, and the f_c is taken as 37.1 MPa. (A_{ffe}) or (F_{fe}) is the applied pre-tension load for each specimen. The load on the rod (A_{ff}) or (F_f) was assumed to be developed once the joint started to open, which was extracted from Fig. 5. For this purpose, the joint opening load was first identified (Fig. 5c). When the opening exceeded 2 mm, the load is selected, then the corresponding deflection to that load was selected from (Fig. 5a), and finally, the axial load for that deflection was extracted from (Fig. 5b). These values have been indicated in (Table 3).

It is evident that the axial load in the GFRP rod is increasing linearly, and with an almost similar slope, for all levels of post-tensioning (Fig. 5b). This indicates that as long as the segments in the joint are in contact with each other (and the concrete on top is not crushed), the rod's load increment is linearly elastic. However, when the joint is opened, the axial load increment decreases as the initial post-tension increases (Table 3), hence, S0-EXP had the highest load increment due to the highest deflection associated with the initial concrete crushing and S42-EXP had the lowest axial load increment.

After the joint opening, the compressive crushing of the concrete in the upper part of the joint was observed. The joint opening of the decks occurred at different levels of applied loading (Fig. 5c). These loads coincide with a load at which the strain increased in the rod (Fig. 5d). For specimen S0-EXP, the absence of post-tension force caused a sudden opening in the transition phase (opening stage), which occurred at a higher rate, in which at 5 kN the joint opened almost 7 mm. This was due to the small friction between the segments and low resistance against opening. In contrast, increasing the initial post-tension force enhanced the behaviour of the joint and increased and resulted in a reduction in the joint opening. The compressive stress between the segments induced by post-tensioning can also enhance shear strength by increasing the compression depth and contact between the segments' surfaces at the joint. The increase in the compression depth can provide higher friction and enhance the shear capacity of the joint interface. This

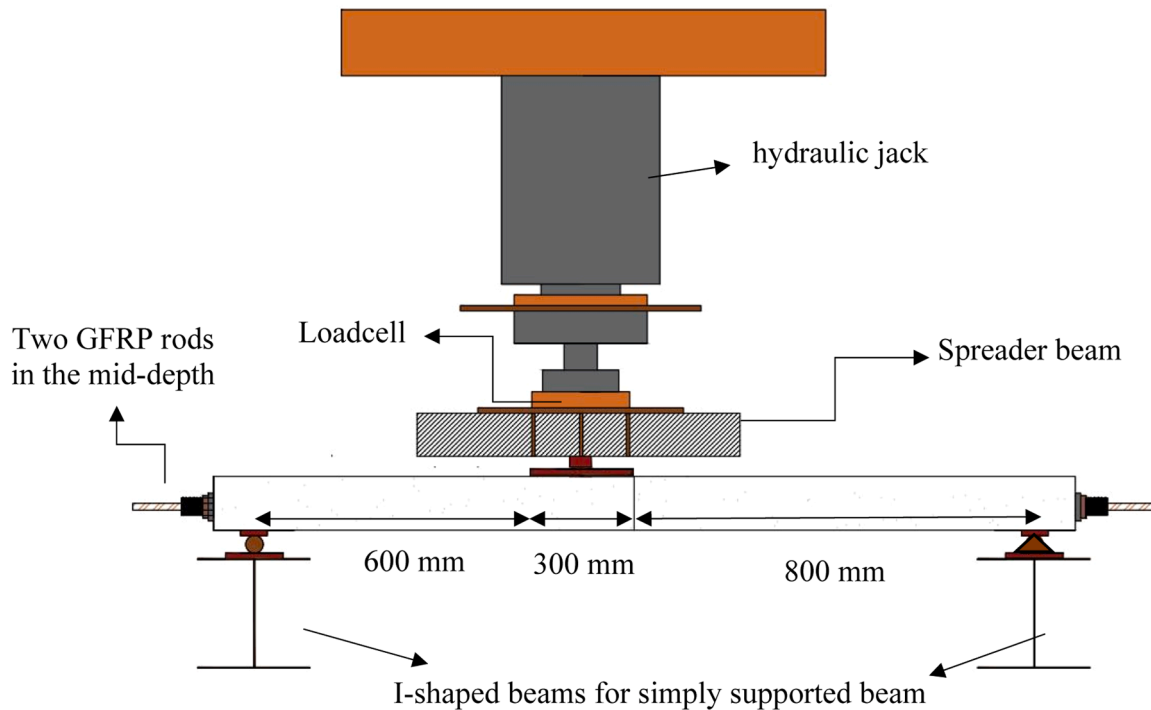


Fig. 3. Schematic view of test setup.

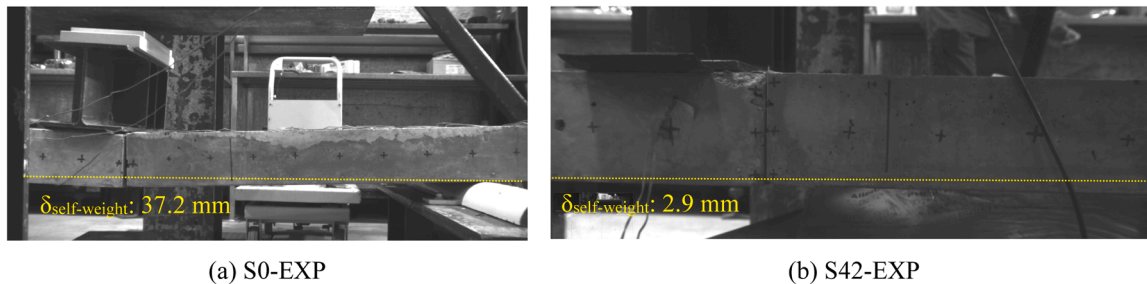


Fig. 4. Self-weight deflection.

was observed in the results of Niwa et al. [51] regarding the effect of surface roughness on the shear capacity of the segmental concrete slab. In their result, concrete slabs with a smoother surface and less friction have 63.9 % lower shear capacity compared to rough ones, and they concluded that the compressive stress in the joint, between the segments, can allow the frictional forces to become established.

As the progressive concrete crushing continued, an abrupt drop in the load-carrying capacity (Fig. 5a) as well as in the applied load-joint opening characteristic (Fig. 5c) of the segmental deck was observed. This drop in load is attributed to the interlaminar shear failure of the rod and the complete concrete crushing in the vicinity of the loading point and joint. This failure behaviour shows that the interface of the joint highly influences the ultimate shear strength of a segmental deck, with concrete compressive strength playing a pivotal role.

The neutral axis depth was calculated and reported in Table 4 to understand its effect on the FRP-reinforced segmental deck's load-carrying behaviour with different initial post-tensioning levels. The theoretical moment was calculated with (Eq. 3) here the rod's depth (d) is equal to 62.5 mm and a is the calculated depth of the equivalent compression block (equal to $\beta_1 c$).

$$M_{cc} = 2(F_f + F_{fe}) \left(d - \frac{a}{2} \right) \quad (3)$$

The comparison between the theoretical moment from section

analysis and the applied bending moment indicates that the hand-tight post-tensioning rod has the highest discrepancy of around 30 %. This high difference can be attributed to the method used for calculating the compression depth and compressive strength in the formula, which was based on the average compressive strength. To obtain the f'_c , the presence of a 17 % difference between the standard deviation (6.2 MPa) and the average value (37.1 MPa) might contribute to this discrepancy, as it affected the neutral axis depth. Increasing the initial level of post-tensioning makes the segments more integrated, reducing the discrepancy between theoretical and applied bending moments.

3.2. Load-strain behaviour

The load-strain behaviour is assessed by the strain gauge attached to the rod between the loading point and joint and at the internal reinforcement in the compression zone (IRC). A comparison between S0-Rod, S21-Rod, S32-Rod, and S42-Rod shows that at the same applied load level, increasing the initial post-tensioning reduces the rod's stress. This also explains the higher midspan deflection of segmental decks with lower than higher levels of post-tensioning in the GFRP rod. At an applied load of 25 kN, the strain in S0, S21, S32, and S42 is 3400 $\mu\epsilon$ (39 % of the anchor strength), 2400 $\mu\epsilon$ (27 % of the anchor strength), 1000 $\mu\epsilon$ (11 % of the anchor strength), and 600 $\mu\epsilon$ (7 % of the anchor strength), respectively. Moreover, there is no strain on the rod when the

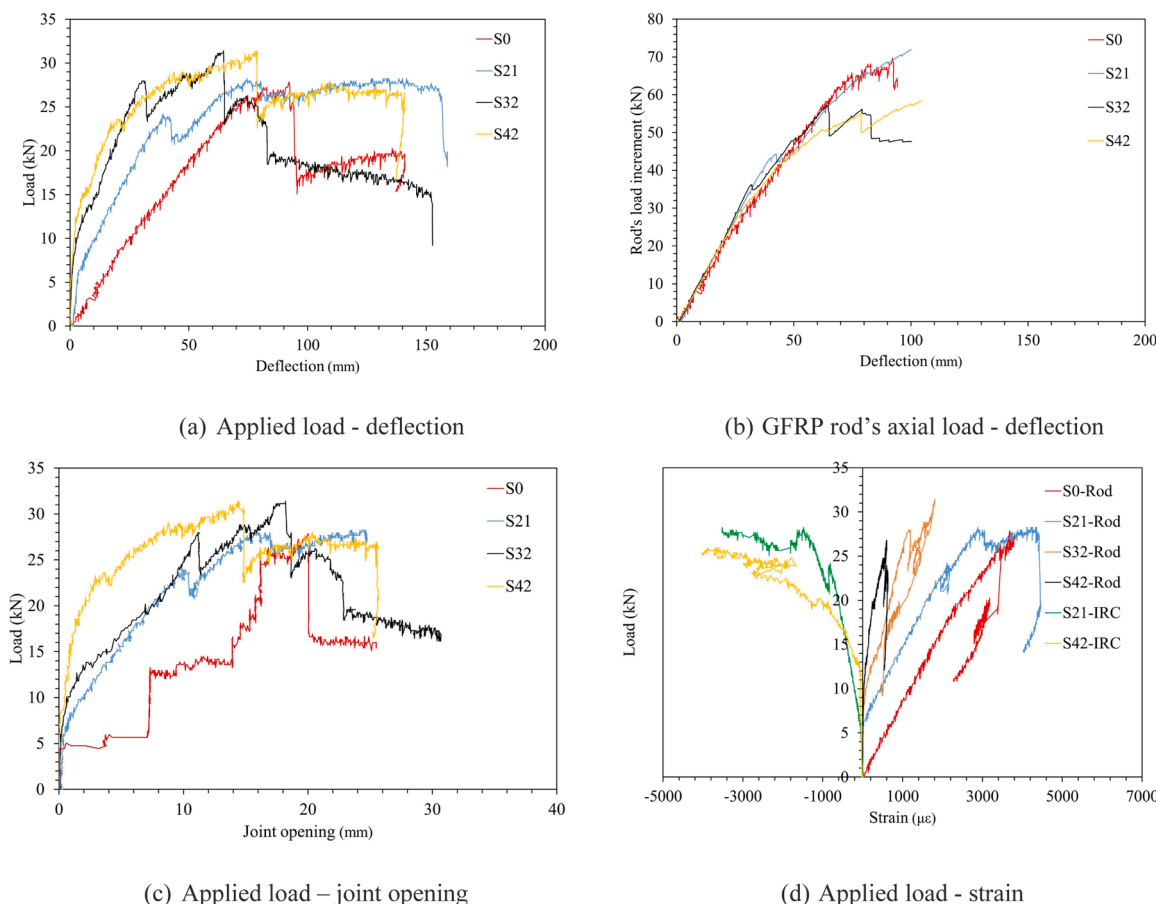


Fig. 5. Experimental results.

Table 3

Neutral axis- initial stiffness relation before joint opening.

Specimen	Rod's load (kN)	Initial post-tensioning (kN)	Neutral axis depth (mm)	Initial stiffness (kN/mm)
S0-EXP	12.7	0	1.1	0.3
S21-EXP	4.5	21	3.9	1.2
S32-EXP	2.5	32	5.4	2.4
S42-EXP	1.3	43	6.9	2.9

joint is closed and starts to increase as the joint opens. The progression of the post-tensioning load shown in (Fig. 5c), can also be correlated with the joint opening. Considering the 5.7 kN and 10 kN applied loads, S21-IRC and S42-IRC started to increase in the negative direction. In the same way, the measured strain in the rod near the joint began to increase. This verifies the mechanism of compression at the top and opening at the bottom of the joint. This linear increase continued until the concrete crushing started. From this point entering the load associated with the ultimate load-carrying capacity, the non-linear behaviour was observed. At this stage, the strain exceeds 0.003, which indicates the strain for concrete crushing ACI440.1 R-15 [50].

Table 4

Compression depth when the concrete crushes.

Specimen	Rod's load (kN)	Initial post-tensioning (kN)	Neutral axis depth (mm)	Theoretical moment (kN.m)	Applied moment (kN.m)	Error (%)
S0-EXP	65	0	8.9	7.2	9.4	30.7
S21-EXP	61	21.6	11.3	8.8	9.9	11.8
S32-EXP	57	32.1	12.2	9.4	10	6.2
S42-EXP	53	42.9	13.1	10	9.8	1.9

3.3. Failure behaviour

The segmental deck failed by concrete crushing from the loading point to the joint. This failure is observed in the segmental beam post-tensioned with CFRP tendons [71,72]. The absence of post-tensioning also caused interlaminar shear failure of the internal GFRP rod. This means applying the post-tensioning can eliminate the localized stress on the rod because of high deflection. The concrete crack propagation initiates differently with the post-tension level. Before the joint opening in deck S0, the depth of the contact between the segment was almost 1 mm (or rotating around the sharp corner). As the lower part of the joint opens, concrete crushing initiated 8.9 mm from the top (Fig. 6a), the lowest compression depth among all samples. In contrast, the compression depth in deck S42 opens is around 13.2 mm (Fig. 6b).

In summary, the segmental deck failure mechanism is concentrated at the joint, where concrete undergoes crushing at the top as the joint opens at the bottom. Increasing the initial post-tensioning leads to a reduction in joint opening and an increase in the neutral axis depth. Moreover, failure is followed by interlaminar shear in the GFRP rod in the vicinity of the joint. Increasing the post-tensioning can minimize this failure by decreasing the deflection and creating a more uniform stress

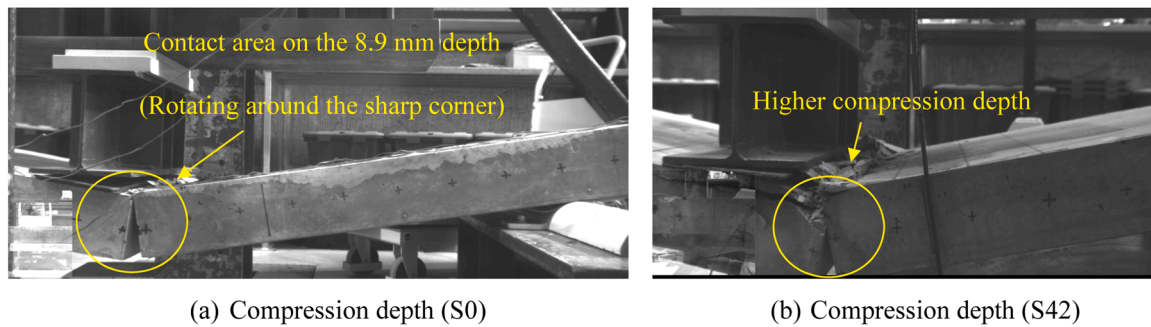


Fig. 6. Failure behaviour.

between the segments. Therefore, a higher level of post-tensioning can potentially cause different behaviour of the joint as the segmental deck behaves more similarly to a monolithic slab; however, applying a higher load and investigation of the other affecting were not possible in the experimental stage, accordingly, creating a finite element model can shed light.

4. Numerical analysis

4.1. General description and assumptions

A three-dimensional model through the Abaqus/CAE software Dassault Systems, 2019 [52] was developed and used for the verification of the experimental results. To simulate the experimental conditions, numerical modelling was carried out using the displacement-controlled approach and a dynamic explicit solver was employed. Previous studies [69,70] showed that dynamic explicit analysis is well-suited for solving intricate contact problems, multi-phase environment, and complex interactions. The concrete used a solid element (C3D8R) with a mesh size of 10 mm, behaved elastic and non-linear in the concrete damage plasticity (CDP) and the equation to define the non-linear behaviour adopted from [53]. The formulation for damage propagation in concrete, both in tension and compression, is adapted from the recommended formula by recent studies [32,33,54]. The internal GFRP bars and rods were simulated with solid elements (C3D8R) with a 25 and 10-mm mesh size for rebar and rod, respectively. The internal rebar has an Elastic behaviour with values reported by Ebrahimzadeh et al., [18]. The rod was assumed to have an orthotropic material. To apply the post-tension force, the GFRP rod is exposed to tension load, equivalent to the load applied in the experimental stage and in the total reaction of the tension load is exposed to the concrete surfaces at both ends as a compression load. The detailed information, formulations, and all assumptions of the boundary conditions can be found in Ebrahimzadeh et al. [39].

4.2. Model validation

The FEM results were verified by comparing them with the failure mechanism loads, displacements and strains obtained from the experimental results. This calibration was conducted for the hand-tight sample (S0), with the lowest post-tension stress, and the deck with the highest initial post-tensioning (S43), as it has the highest initial tension stress on rods. The initial post-tension for other specimens were in between these two decks and were analysed in the previous study [39]. The verification helps to establish a model for further investigation (parametric study) and the stress/ strain distribution in the joint in addition to the failure mechanism can provide a detailed behaviour of the experimental result and comprehension of what couldn't be seen/measured throughout the test e.g., neutral axis depth of the concrete at the joint which calculated based on the theoretical evaluation.

4.2.1. Load-deflection

The effect of post-tensioning on the load-carrying capacity of the segmental deck was analysed up to 80 mm deflection (Fig. 7). It was observed that the specimen without post-tensioning (S0) exhibited linear behaviour, similar to the experimental specimen. In contrast, the specimen with post-tensioning (S43) initially behaved linearly before transitioning to non-linear behaviour associated with concrete crushing. A discrepancy was noted between the bending stiffness of the finite element models and the experimental results before joint opening, similar to the findings reported by Tran et al. [33]. This can be attributed to the imperfections in fitting the post-tensioned segmental deck in the experimental specimens. In addition to this, the differences in how the post-tensioned specimens are simulated and the estimation of the friction coefficient between the segments may contribute to the discrepancy. Unlike in the experimental setup where the post-tension force was transmitted through steel plates and load cells, in the finite element model, it was applied uniformly to both end sides, which could have a different effect on the overall behaviour. The ultimate load-carrying capacity of the S43-FEA is very close to the S43-EXP (30 kN). The difference in a lower deflection can be attributed to the lower diameter of the hole in the segments, compared to an experimental specimen. For simplicity, the PCV is excluded, and its thickness is included as a concrete material.

4.2.2. Strain behaviour

The detailed load-strain behaviour was analysed based on the behaviour of concrete elements in the joint. In both models, the concrete element located at the topmost part of the joint experienced compression, while the second element did not exhibit clear compression behaviour. This aligns with the calculated compression depth ranging from 7.2 to 13.1 mm. In the specimen without post-tensioning (S0), before the joint opening, all elements (located in the sharp corner, over the rod, and in the middle width of the deck) experienced similar strain and stress. However, as the joint opened and concrete crushing progressed, the elements in the corner were exposed to higher stress, likely due to stress concentration at the sharp corner. The elements over the rod (Element 1-Rod) and in the middle (Element 1-Mid) exhibited higher strain as the joint opened further. This suggests that the arrangement of the rods may result in a more uniform stress distribution between them. Another observation is the gradual and steady increase in strain until just before reaching 15 kN of load, with a limited strain increase (below $500 \mu\epsilon$). Subsequently, there was a higher strain increase until reaching approximately $-3000 \mu\epsilon$, indicating concrete crushing according to ACI440.1 R-15 [50]. Conversely, the strain behaviour in S43 exhibited a more uniform increase in strain (Fig. 8c) and a steep increase with a very high slope (Fig. 8d) before the joint opening (5 kN). Upon joint opening, the strain in the concrete continued to increase until reaching 30 kN, although, within this stage, several drops were observed. It was noted that the concrete element at the interface of the GFRP rod (around the hole) experienced very high stress (Fig. 9a and Fig. 9c), leading to the failure of the element. This contact in the experimental specimens

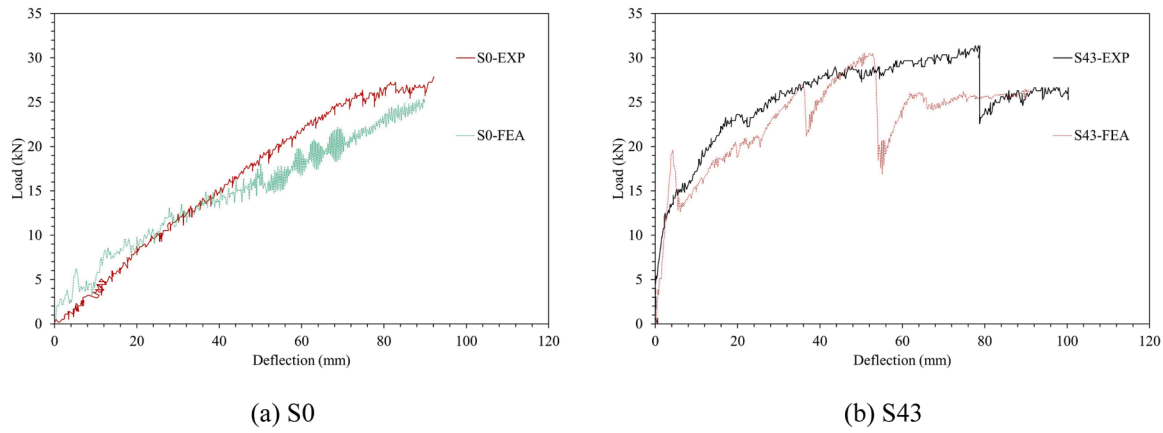


Fig. 7. Model calibration (load-deflection).

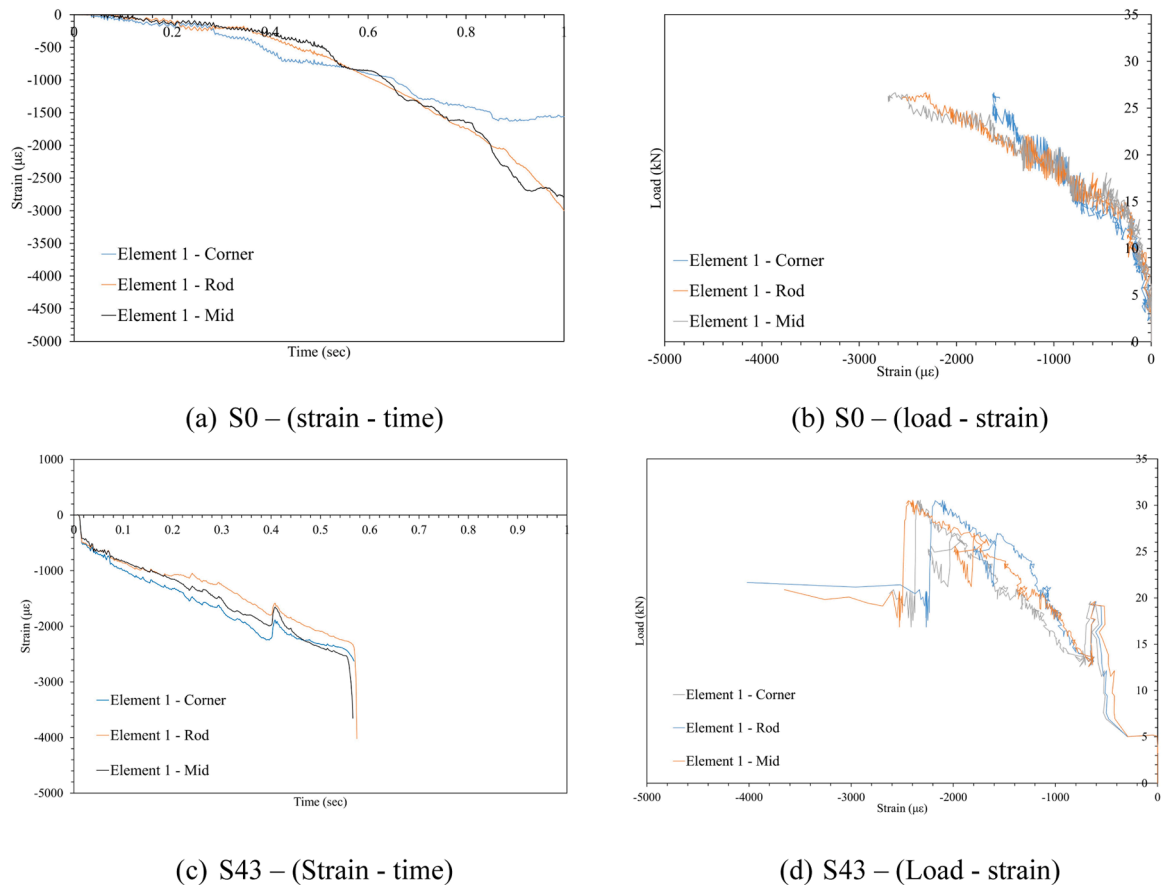


Fig. 8. Concrete strain behaviour in joint.

resulted in interlaminar shear failure of the GFRP rod (Fig. 9b).

4.2.3. Failure mechanism

Fig. 9 illustrates the failure mechanism in the concrete before the joint opening and on the GFRP rod at the ultimate stage. At the same load level (5 kN), the compression stress in S0 (Fig. 9a) is concentrated at the sharp corner of the segment, whereas in S43 (Fig. 9c), it extends throughout the entire depth of the first element. In the ultimate stage for both cases, the rod is subjected to high stress in the joint (Fig. 9b). However, it is distributed more uniformly in S43, indicating the tensile stress due to pre-tensioning prevented the localized stress on the rod and potentially reduced the interlaminar shear failure (Fig. 9d).

The stress distribution analysis at the joint during cracking in specimens S0 and S43 reveals differences in the rod/concrete interaction (Fig. 10). For S0, under a 5 kN load and 9.5 mm deflection, the compression bending stress was concentrated at the sharp corners of the concrete segment, leading to localized stress (Fig. 10a). In contrast, S43, with a 6.5 kN load and 3.5 mm deflection, exhibited a more uniform stress distribution through the width of the segment, due to the pre-tension force (Fig. 10b), allowing it to expose to a higher compressive stress of 4.2 MPa before crushing, compared to 2 MPa in S0, almost a 110 % improvement. The GFRP rod/concrete interface in S0 showed high compressive stress on the rod. However, the pre-tension on the rod alleviated the stress in the rod interface (37.5 % lower stress at S43),

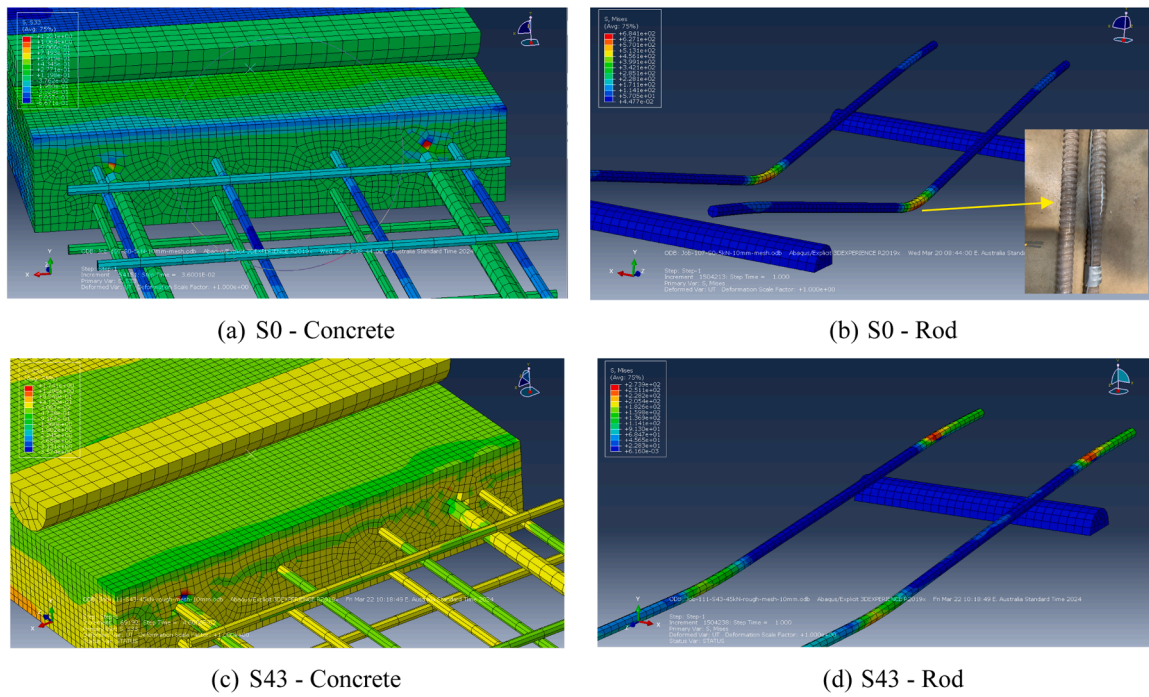


Fig. 9. Failure mechanism.

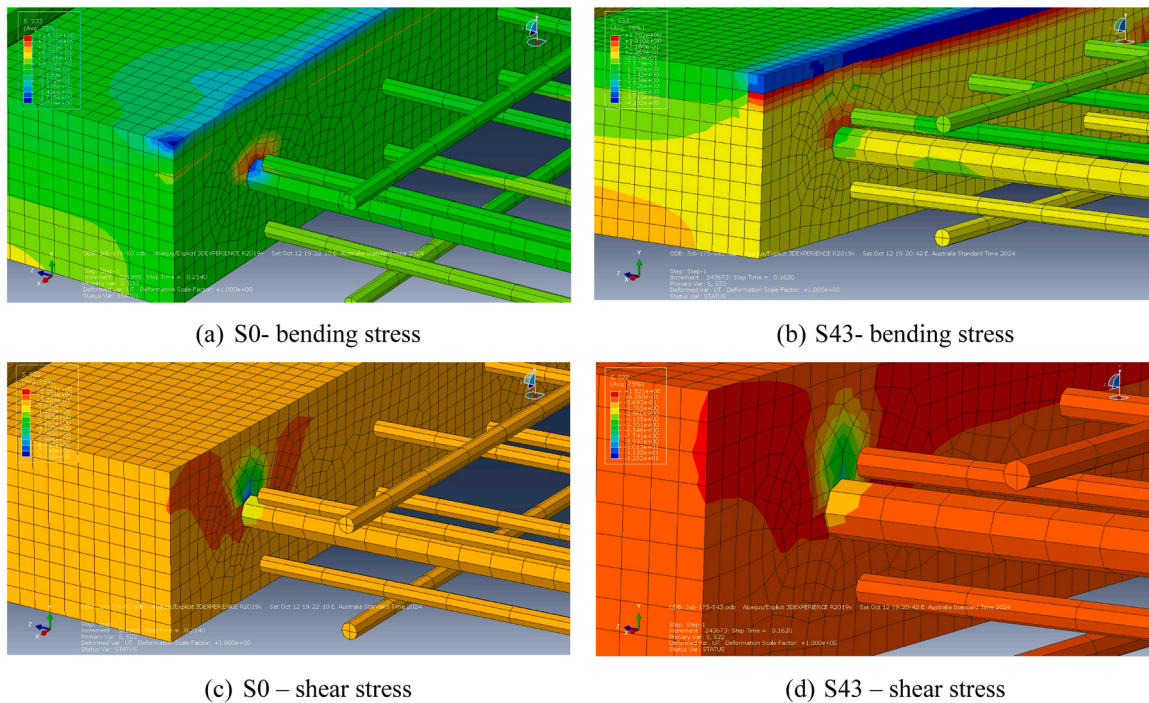


Fig. 10. Stress at the joint cracking.

which is consistent with the test result as interlaminar shear was observed in S0 while in S43 the concrete crushing was the governed failure mechanism. The shear stress distribution at the joint in the rod/concrete interface in S0 (Fig. 10c) shows a maximum shear stress of 8.7 MPa on the concrete, while at the edge of the concrete in S43 (Fig. 10d), the shear stress is reduced to about 5.35 MPa. In both cases, stress concentration in the edge of concrete and rod is observed. Given the rectangular cross-section of the segmental deck, the maximum calculated shear stress at this applied load is approximately 0.1 MPa and

it is occurring in the neutral axis. However, the shear stress distribution is different in segmental system. The higher observed shear stresses indicate that the load transfer occurs primarily through the joint, following a path from the top portion of the GFRP rod and the concrete/rod edge exposes to a high shear stress. Additionally, the concrete elements located at the joint, those on the top part of the segment, are subjected to nearly similar induced shear stresses in both decks.

5. Parametric study

Once the detailed behaviour is investigated, and the model based on the experimental result is calibrated parametric study can be performed. According to the Australian design guideline AS 4997–2005 [55], the design requirements of the marine structures based on serviceability should be limited to a maximum deflection of $(L/150)$. An investigation in the serviceability range helps the design recommendation be useful in real practice as the high level of deflection in the segmental pontoon deck cannot provide them an ideal alternative to the monolithic one.

Accordingly, a parametric study is implemented to investigate the effect of the different affecting parameters including loading point, concrete properties, mesh size, post-tension force, interlock, rod's depth and number, internal reinforcement, and deck's geometry to identify approaches to improve the overall stiffness and load-carrying capacity of GFRP-reinforced segmental pontoon decks within the serviceability range.

5.1. Location of the loading point

The loading applied directly on the joint presents a critical scenario for the segmental deck post-tensioned with GFRP rods. Due to feasibility constraints in the experimental setup, the load was instead applied 150 mm away from the joint, and the FE model was accordingly calibrated (S43-FEA). Moreover, to avoid arching action and to understand the shear transferring mechanism across the joint, the load is applied at a distance from the joint. Subsequently, to investigate other loading scenarios, simulations were conducted also for loading directly on the joints (S43-FEA-L0) as well as at a distance of 750 mm from the joints (S43-FEA-L750), as depicted in (Fig. 11). As anticipated, loading directly on the joint reduced load-carrying capacity compared to S43-FEA. Observations indicated concrete compression at the top of the joint and an opening at the bottom. Shifting the loading point further away from the joint led to a transition in behaviour from segmental to monolithic; accordingly, the behaviour changed from linear (in S43-FEA-L0) to a combination of linear (before compression beneath the loading point) and non-linear stage (after compression). In S43-FEA-L750, not only did the stiffness and load-carrying capacity increase, but the failure mechanism also shifted towards the compression zone at the loading point. Compression within the joint during loading was observed; however, heightened arch action caused load transfer to the support in the shear span, diminishing the prominence of the joint's presence. While the

effect of span-to-depth ratio on GFRP concrete monolithic decks has been studied previously by Ebrahimpzadeh et al. [18], the comparison regarding loading proximity to the joint remains less understood. Nonetheless, a study on segmental beams prestressed by external steel tendons, such as that by Yuan et al. [31], demonstrated a 35 % increase in load-carrying capacity when altering the span-to-depth ratio from 30.5 to 17.9. In their study, the load applied in both scenarios is far from the joint, and the failure based on the span-to-depth ratio range is considered flexural in both cases.

5.2. Concrete properties

The influence of concrete properties can be divided into two categories. Plasticity parameters can represent the effect of the parameters used on the behaviour of concrete in the numerical model. Among plasticity parameters, studies [32,54,56–58] selected almost similar values for eccentricity, viscosity parameter, and K_c for concrete. $(\frac{\sigma_{bc}}{\sigma_{c0}})$ is also calculated from Papanikolaou & Kappos [59] which is very close to the value selected in the mentioned studies.

The angle of dilation (ψ), caused by shear in the material micro-structure, indicates the internal friction angle and controls plastic volumetric strain [60], and varies across different studies in the literature. While many studies [33,54,56,57] suggest a range of 31° to 35° , with recommended values falling between 30° and 40° [61], there are instances of wider ranges used for specific concrete types. For example, ultra-high-performance concrete may have a dilation angle as low as 15° [62], while some studies suggest values as high as 55° [63]. To explore the impact of this parameter, two segmental decks without initial post-tension force in the rod were modelled and compared. Additionally, the guidelines set by the DTMR-2019 [40] limit the use of concrete with a compressive strength below 50 MPa. However, the mean compressive strength of the tested segments in this study was 37.1 MPa. Therefore, the effect of using concrete with a compressive strength of 50 MPa, the basic permitted concrete in Queensland, was investigated. Furthermore, high-strength concrete can range from 50 to 100 MPa [64], prompting an examination of the effects of higher concrete compressive strength, such as 75 MPa.

5.2.1. Dilation angle

Changing the angle of dilation from 15° to 55° resulted in a 9 % increase in bending stiffness and a 4 % increase in load-carrying capacity at the serviceability limit (Fig. 12a). Additionally, the segmental deck

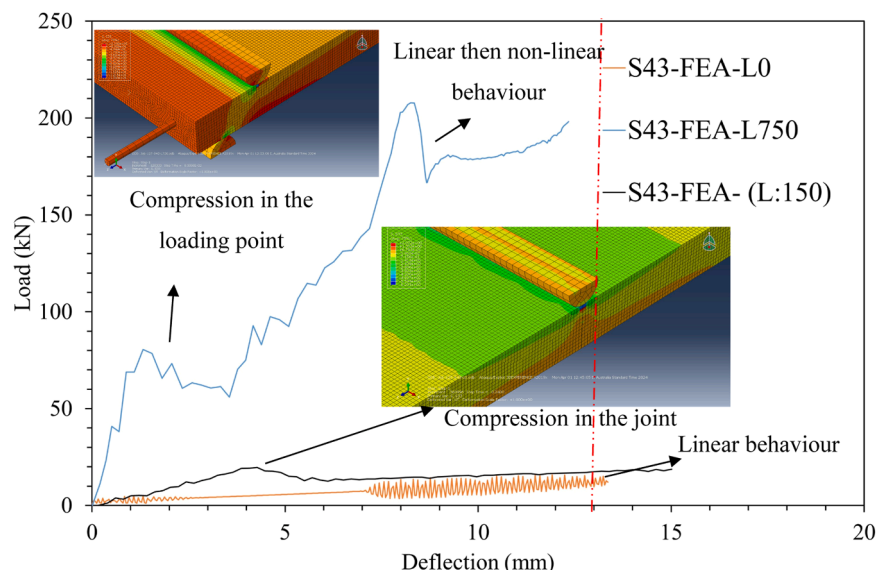


Fig. 11. Effect of the loading point locations.

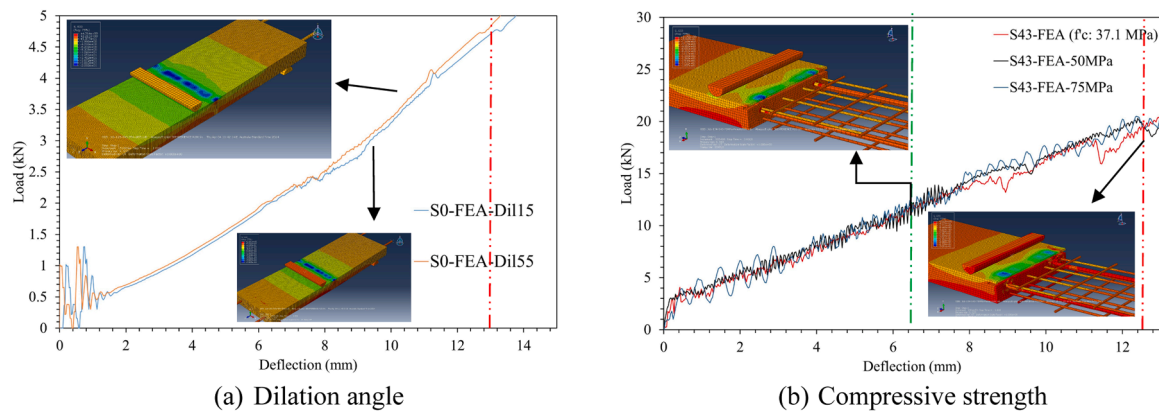


Fig. 12. Influence of the concrete properties.

modelled with a dilation angle of 55° exhibited a 3 % higher initial bending stiffness than the one with a dilation angle of 33° (S0-FEA). However, it is worth noting that the effect of the dilation angle is more pronounced in monolithic beams. For instance, in the numerical modelling of monolithic concrete beams [60], changing the dilation angle from 15 to 55° increased the maximum load-carrying capacity from 140 to 300 kN. This emphasises that in monolithic beams, where the failure mechanism is governed by tension-control mode, the dilation angle plays a critical role in model calibration. Conversely, in segmental concrete decks where the failure is primarily governed by compression in the joint, the effect of the dilation angle is less important.

5.2.2. Concrete compressive strength

Changing the compressive strength of concrete from 37.1 to 75 MPa did not affect the segmental deck's initial stiffness or load-carrying capacity up to an applied load of 12.8 kN (7.9 mm deflection). This suggests that the concrete properties do not significantly impact the behaviour of the segmental deck as long as the behaviour remains linear. This finding aligns with Le et al. [30], who reported similar results with internal steel tendons in T-shaped segmental beams. However, at the load point of 12.8 kN, the concrete element in the joint crushed (or failed), causing a divergence in the curves (Fig. 12b). Lower concrete strength resulted in a higher reduction in load-carrying capacity. This study focused on the segmental deck's response to the serviceability limit and the failure behaviour in this range was slightly different. While 6 concrete elements failed in both S43-FEA-37.1 and S43-FEA-50MPa models, from the joint to the loading point (equivalent to 60 mm), the extent of concrete failure in the S43-FEA-75MPa model was limited to 5 elements (50 mm). This demonstrates that increasing concrete strength can provide slightly more resistance against compression in the joint, resulting in an improved response. However, the effect of compressive strength when the behaviour of the segmental deck must stay in the permitted serviceability range is not significant.

5.3. Mesh size

Although mesh size can be categorised as a FEM model development rather than a parametric study; however, Raza et al. [65] demonstrated that in monolithic GFRP-reinforced concrete members, a smaller concrete mesh size showed a higher initial stiffness compared to experimental results. Moreover, the smaller mesh size offers improved non-linear behaviour within the 2–7 mm deflection range. It is predicted that smaller mesh sizes offer better accuracy, yet in terms of optimization, it is more precise to consider the time and material consumed to achieve the result and compare it with the accuracy in the segmental concrete system. Accordingly, S0-FEA with three different concrete mesh sizes (5, 30, and 10 mm, the reference one) was simulated and 6 processors were allocated for each model to perform the numerical

analysis. Accordingly, 30, 10, and 5 mm concrete mesh sizes were simulated in 7.48, 39.9, and 470 h, respectively. The reduction in mesh size has been shown to increase bending stiffness, similar to monolithic concrete members, yet a more significant impact is noted in achieving a refined curve with reduced fluctuation. Hence, using a mesh size of at least 10 mm is suggested. Although a lower mesh size did not directly influence the load-displacement curve, it did enhance the failure mechanism and compression between the segments (Fig. 13). However, this improvement comes at the expense of a longer duration, which may not be practical.

5.4. Level of post-tensioning in the rod

In the experimental program, higher initial prestressing levels were challenging to achieve, though post-tensioning did improve performance. Therefore, FEM was used to evaluate the effect of applying higher levels of post-tensioning. Given that the maximum tensile strength of the anchor was 328 kN (756.8 MPa), two specimens with initial prestressing of 70 and 100 kN load on each rod (161 and 230 MPa, respectively) were evaluated. These prestressing loads remain within 40 % of the ultimate tensile strength of the GFRP rod ACI 440.4 R-04 [49]. It was observed during the experimental program that the axial load in the rod, regardless of the level of post-tensioning, increased up to 13 kN within the range of serviceability limits (Fig. 5b). Hence, those levels of prestressing will not be problematic for exceeding the strength of the end anchor. Increasing the initial prestressing to 161 MPa and 230 MPa boosted the initial stiffness, achieving improvements 9 and 13.5 times greater than those of the hand-tightened experimental specimen (S0-EXP). This improvement was both anticipated and observed in the experimental stage of the current study, as well as in previous studies of post-tensioned segmental beams with steel tendons [30] and numerical simulations of CFRP tendons [32]. Comparing the two post-tensioned specimens, raising the initial post-tensioning from 161 MPa (21 % of the anchor's tensile strength) to 230 MPa (a 42 % increase) resulted in a 48 % increase in bending stiffness. This is in line with the results of Tran et al. [32], where a 66 % increase in the initial prestressing of the CFRP tendons led to a 67 % increase in initial bending stiffness. However, the impact on failure behaviour was more pronounced, as S100-FEA exhibited behaviour more similar to a monolithic beam. The compression crushing from beneath the loading point to the joint caused a specimen failure and a subsequent drop in load-carrying capacity (Fig. 14). This means a 230 MPa initial prestressing on rods improved the bending stiffness and load-carrying capacity in the permitted serviceability range; however, due to reduced ductility, the specimen failed in a lower deflection. Le et al. [30] observed similar behaviour in the failure mechanism of steel tendons, noting a shift from yielding the steel tendon to failure due to compression.

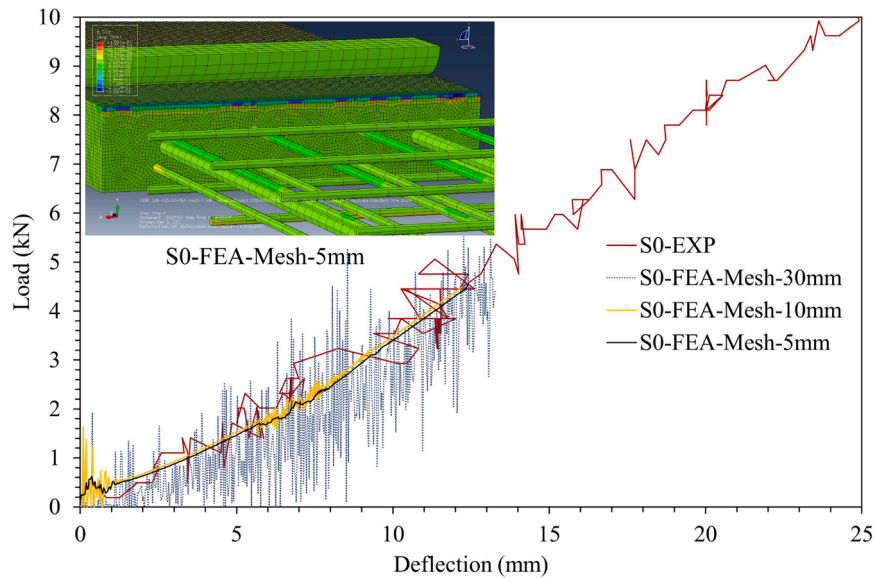


Fig. 13. Influence of the mesh size.

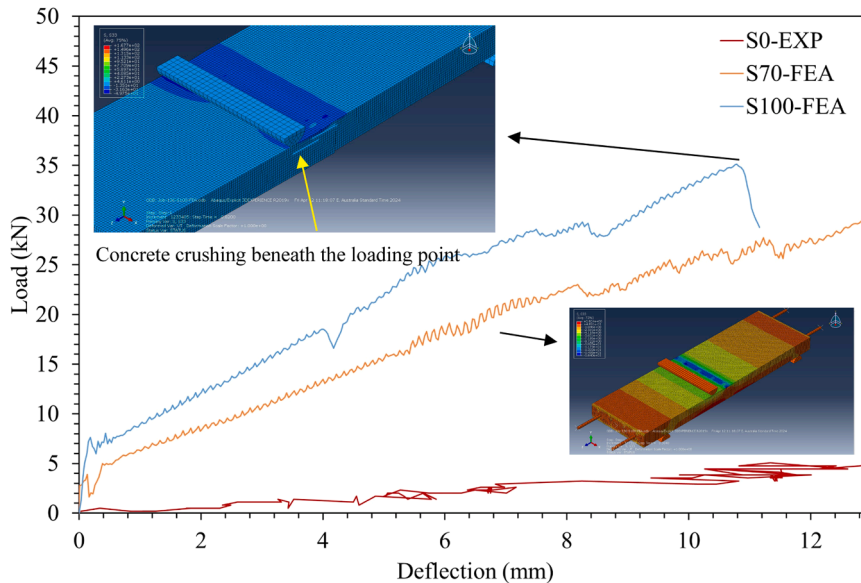


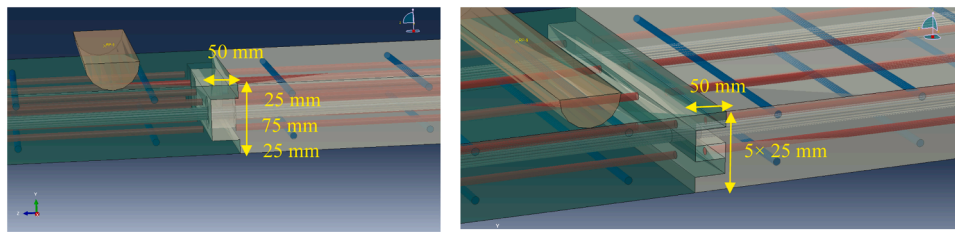
Fig. 14. Higher level of post-tensioning.

5.5. Interlock in joint

The interlock effect in joints was investigated in the cases of single (Fig. 15a) and multiple interlocks (Fig. 15b). In both scenarios, the length of the segments is still 1 m; however, in the joint and at a distance of 50 mm between the segments, the interlock system is considered. The findings reveal that implementing a single interlock enhances bending stiffness by approximately 90 % at a hand-tight level of post-tensioning. On the other hand, multiple interlocks do not offer any performance enhancement. In the single interlock setup, the top part of the interlock provided resistance initially which caused a higher load-carrying capacity but when the interlock failed the behaviour became similar to S0-EXP. Although the S0-FEA-SI model exhibited significantly greater rigidity than the S0-EXP model, its behaviour approached that of a deck without any interlocks as deflection increased. However, at the maximum serviceability limit, the applied force was still 20 % higher due to the presence of interlock in the bottom part, resisting the joint opening (Fig. 15c). It can be concluded that S0-FEA-SI causes

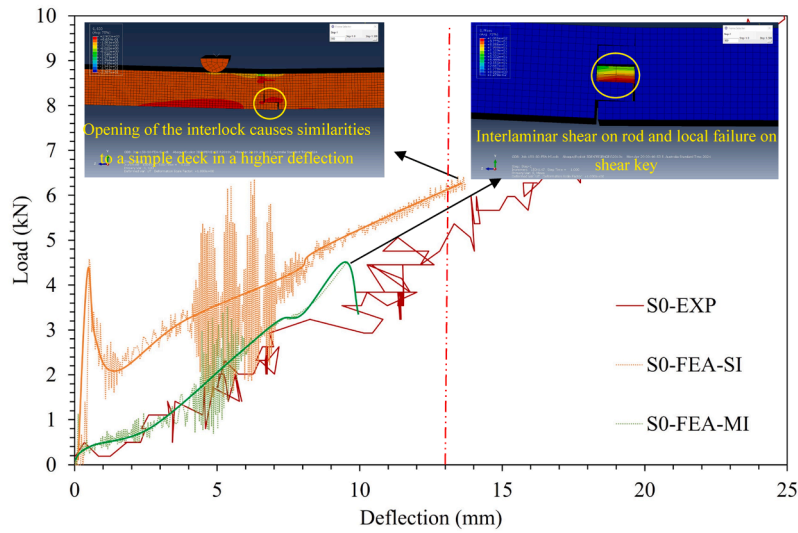
compression in the top part of the joint and opening along the shear key which potentially causes shearing of the key at the joint in a higher deflection. This behaviour is observed in the numerical modelling of the single shear-key test [66], in which compression failure of the flange was the dominant failure mechanism. Conversely in multi-interlock, due to the internal rod, using a continuous middle interlock as a shear key with a hole is not feasible. As a result, a discontinuous middle interlock leads to an inappropriate interlock and very high stress at the interface between the GFRP rod and concrete, causing the shear key (beneath the rod) to fail at a deflection of 9 mm.

Given that the interlock system functions by offering additional resistance against applied loads, it is crucial to explore its effects with post-tensioning and at deflections exceeding the serviceability limit. Thus, the specimens were simulated again with an applied load of 21 kN on each rod (comparable with S21-EXP) and a deflection of 40 mm (Fig. 15d). Applying post-tensioning did not significantly alter the load-carrying capacity or failure mechanism of the S21-FEA-SI model, with evident compression observed on the top part of the interlock. Although

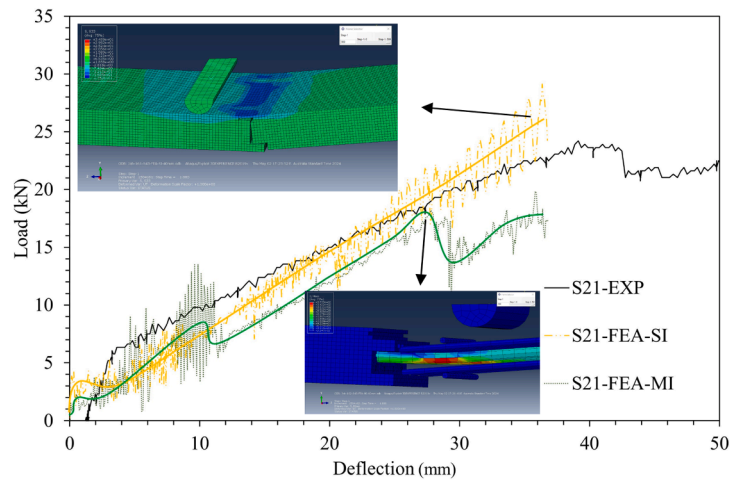


(a) S0-FEA-SI

(b) S0-FEA-MI



(c) Load-displacement



(d) Load-displacement

Fig. 15. Interlock in joint.

the load-carrying capacity slightly improved after a 20 mm deflection due to the interlock system, the overall behaviour remained relatively consistent. Conversely, the S21-FEA-MI model exhibited high stress on the GFRP rod (Fig. 15d), leading to the failure of the concrete element surrounding the rod, as well as the top shear key. According to this section, the incorporation of the shear key and interlock system, due to complexity at construction, presence of the internal GFRP rod, and negligible influence on the behaviour of the segmental pontoon deck is not recommended.

5.5.1. Number of post-tension rod

Previous studies [29,30,32–34] have demonstrated the beneficial

impact of the tendon reinforcement ratio on the flexural-shear performance of segmental concrete beams. Additionally, the influence of the internal reinforcement ratio has been examined [18,26]. This section evaluates the effect of the internal GFRP rod's reinforcement ratio without post-tensioning. This approach differs from previous studies because it involves the absence of initial prestressing in segmental beams and the lack of bonding between the rod and concrete, distinguishing it from monolithic constructions. Therefore, the influence of the number of GFRP rods on the segmental deck's performance can be evaluated by comparing the S0-FEA model with S0-FEA-3rods (Fig. 16), which varies the reinforcement ratio (ρ_{rod}) of the GFRP rods by 50 % while keeping the effective depth the same in both models.

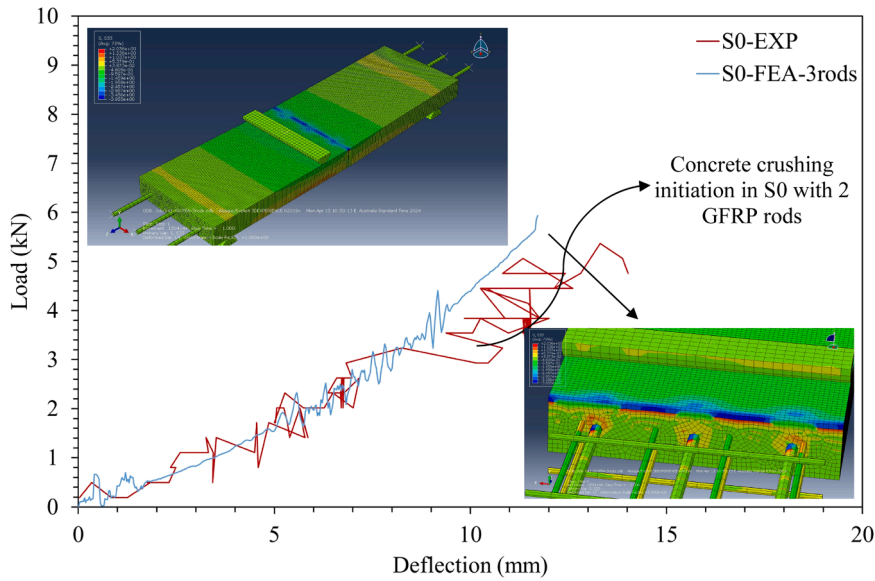


Fig. 16. Effect of the rod's reinforcement ratio.

Adding a third GFRP rod in the mid-section did not change the initial stiffness of the segmental deck. This is likely due to the absence of initial post-tensioning; however, beyond 8 mm of deflection, the load-displacement curves begin to diverge. At this point, the concrete at a joint in the S0 specimen starts to crash, resulting in a decreased load-carrying capacity. In contrast, the concrete in the S0-FEA-3rods specimen remains undamaged within the serviceability range. The higher reinforcement ratio and reduced spacing between the rods lead to an increased load-carrying capacity of 25 % at 13 mm deflection while maintaining intact concrete and ensuring more uniform compression between the segments. This non-linear relation between the reinforcement ratio and capacity is observed by El-Naqeeb et al. [27] as the ratio increased by 25 % the capacity increased by 9 %.

5.6. Rod's depth

GFRP eliminates the need for the conservative 65 mm minimum concrete cover over internal reinforcement to prevent corrosion, as specified in AS 3600–2018 [44]. This not only adds flexibility to GFRP-reinforced concrete design but also provides a chance for further investigations into optimisation. For instance, Ebrahimzadeh et al. [18] explored the influence of effective depth on the performance of monolithic concrete slabs. Their findings indicated that a 36 % increase in effective depth (from 62.5 to 93 mm) enhanced the initial bending stiffness and cracking moment by 26 %. The effects of rod arrangement

have yet to be explored in segmental decks, where there is no bond between the concrete and the FRP rods. Consequently, the effective depth of the segmental deck was increased to 93 mm from the top (Fig. 17a), similar to the approach taken by Ebrahimzadeh et al. [18]. In contrast to the addition of a third rod, increasing the depth of the rod resulted in a 25 % improvement in the initial stiffness, similar to the behaviour observed in monolithic slabs. The load-carrying capacity and bending moment within the serviceability range also experienced a 26 % increase. This enhancement can be attributed to the more uniform compression between the segments within the joint and a greater compression depth, extending beyond the second concrete element (Fig. 17b).

5.7. Internal GFRP reinforcement

The joint discontinuity in segmental concrete decks prevents the internal reinforcement from significantly contributing to the load-bearing capacity, as evidenced by the negligible strain increase in internal reinforcement during testing. Maintaining internal reinforcement is crucial for structural integrity and preventing local failures due to dynamic impacts, such as debris or small vessel strikes. Initially, the rods were positioned mid-depth (62.5 mm from the top). Adjusting the GFRP rod's depth to 93 mm from the top allows optimisation. In the original segment, transverse and longitudinal reinforcement ratios were 1 % and 1.68 %, respectively. This section introduced three other internal

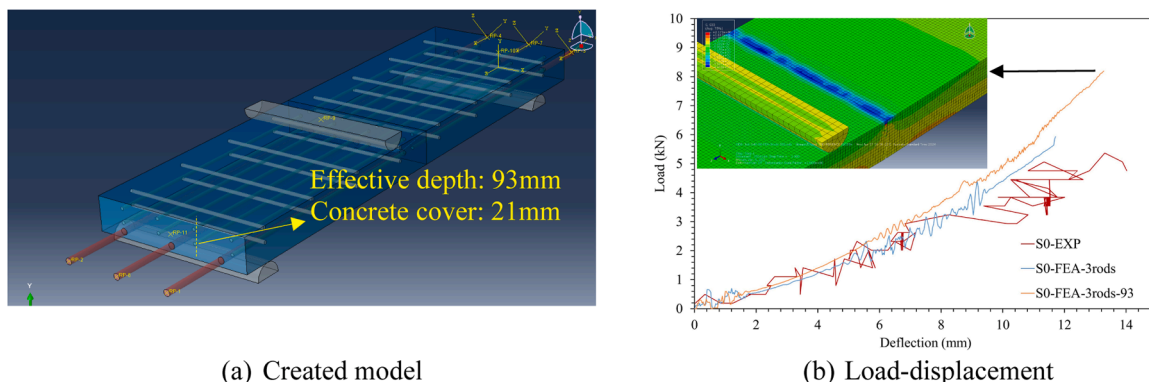


Fig. 17. Effect of the rod's depth.

reinforcement scenarios: S0-FEA-SLM features a single layer of GFRP rebar at mid-depth, resulting in transverse and longitudinal reinforcement ratios of 0.76 % and 1.28 %, respectively. S0-FEA-SLT retains a similar setup but positions the GFRP mesh 30 mm from the top, providing a concrete cover of 25 mm. Finally, S0-FEA-SLTC includes an additional transverse rebar near the joint to assess the impact of the additional transverse rebar on the segmental deck's response.

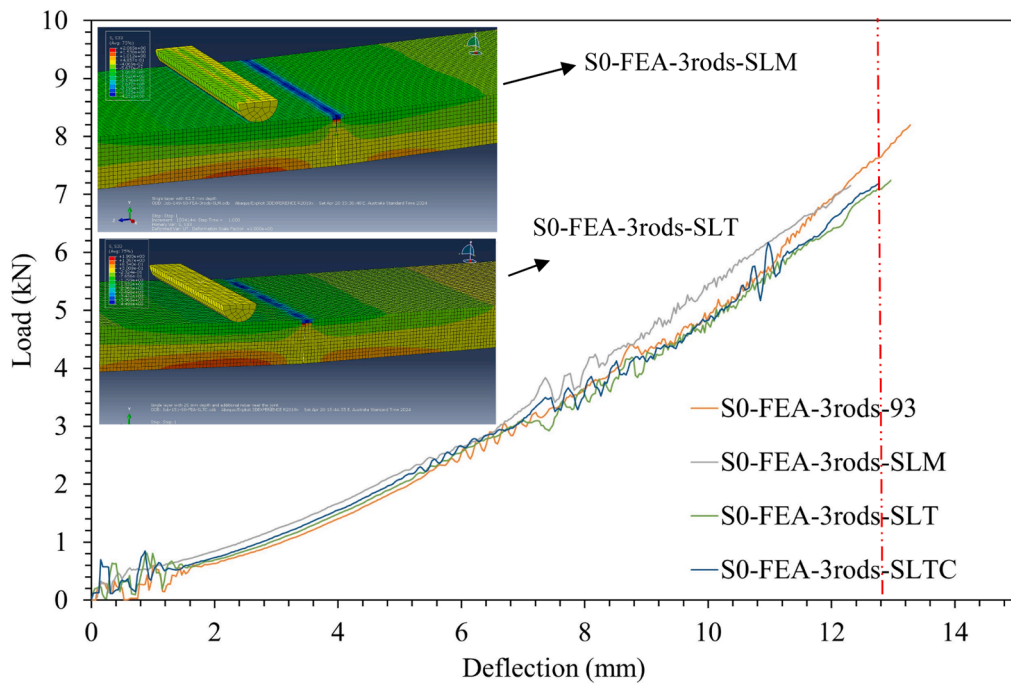
Changing the reinforcement arrangement did not significantly alter the load-carrying capacity of the specimens within the serviceability range (Fig. 18a), even with a 24 % reduction in both the transverse and longitudinal reinforcement ratios for each segment. This suggests that optimizing the internal reinforcement ratio to 0.76 % (using a single layer at mid-depth) and compensating with an additional rod could be a viable strategy for minimizing GFRP rebar usage, particularly in scenarios where segmental deck deflection is constrained (e.g., boat ramps).

While the analysis did not extend beyond the serviceability range in this study, understanding the failure behaviour associated with different bar arrangements could be potentially valuable. Hence, further examination of compression in joint and load-carrying capacity in different reinforcement scenarios is conducted for S0-FEA-3rods-DL (double

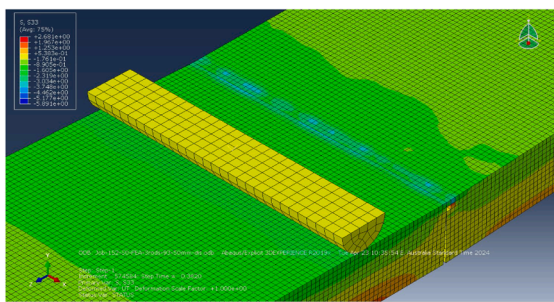
layer) and S0-FEA-3rods-SLM (single layer in the mid-depth) specimens. It has been noted that employing either a double layer or a single layer of reinforcement does not significantly alter the load-carrying capacity when the concrete undergoes non-linear behaviour. Furthermore, in addition to the comparable load-carrying capacity, the bending stress at the joint precisely at the moment of failure of the first element in S0-FEA-3rods-DL is 2.68 MPa (Fig. 18b), exhibiting just a 3 % difference from S0-FEA-3rods-SLM (Fig. 18c). This observation suggests that the internal reinforcement can be reduced to optimize the number of internal rods used in the segmental deck. However, further investigation is suggested, particularly under dynamic impact loading conditions, to ascertain whether altering the reinforcement layer in the segmental deck leads to a significant change in the event of local failure.

5.8. Deck's geometry

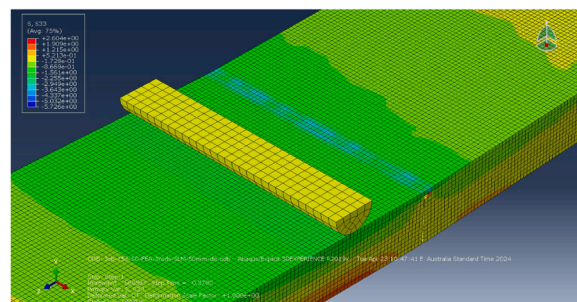
Considering the deck is monolithic and joint does not exist, and according to ACI 440.1 R-15 [50], the cracking moment can be predicted by $(\frac{0.62\lambda\sqrt{f'_c}I_g}{y_t})$ where (f'_c) , (I_g) , and (y_t) are concrete compressive strength, the gross moment of inertia, and the distance from the centroidal axis of



(a) Pre-crack stage



(b) DL



(c) SL

Fig. 18. Effect of the internal rebar arrangement.

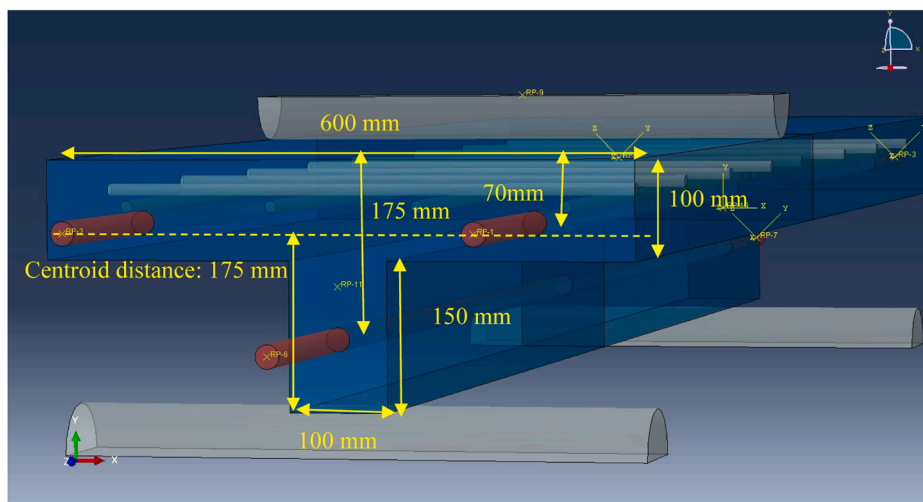
the gross section, respectively. λ is the reduction factor for lightweight concrete which is not applicable in this current study. Moreover, in the equation provided, the effect of the internal reinforcement (in this case GFRP rod) is ignored. Accordingly, by having the same cross-sectional area and increased moment of inertia the possibility of improving the cracking moment by utilising the same amount of material provides further optimisation. Accordingly, the original specimen with a rectangular cross-sectional area has I_g of $9.76E07 \text{ mm}^4$ and S0-FEA-3rods-Tshape, with the same area having a gross moment of inertia of $2.65E08 \text{ mm}^4$. Hence, if the monolithic GFRP-reinforced concrete beam is tested under these scenarios the cracking load of rectangular should be 63 % lower than the T-shape. Knowing this background, the T-shape sample is created (Fig. 19a) and compared with the reference sample with a hand-tight initial post-tensioning.

The results indicate that in the T-shape deck where the load was applied, high compression stress in concrete at the joint is observed showing increasing the depth causes a higher resistance and better load

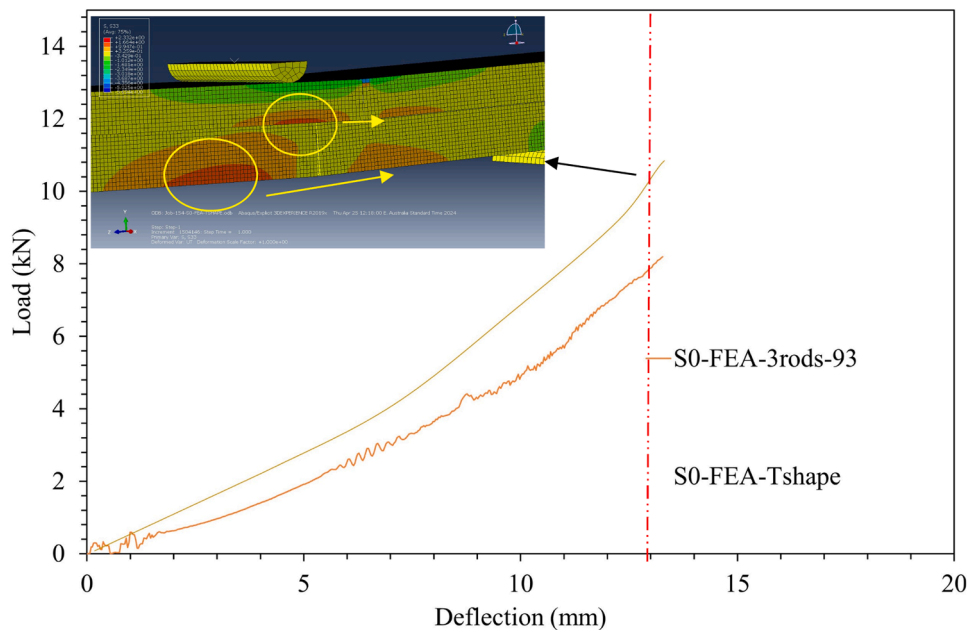
transfer (Fig. 19b). Furthermore, the initial bending stiffness and the cracking moment at 13 mm deflection in the T-shaped segmental beam were 45 % higher than those in the rectangular concrete deck. However, the prediction equation estimated a higher improvement (176 %). This observation suggests that, unlike monolithic concrete beams, the segmental deck, which exhibits an opening of the joint at the bottom and compression at the top, displayed a lower improvement in its flexural strength.

5.9. Modified design

Based on the results of a numerical parametric study, a modified segmental deck design is proposed (Table 5). The design features a concrete compressive strength of 50 MPa, a T-shape cross-sectional area, and incorporates 3 internal GFRP rods. The total initial post-tensioning force is set at 100 kN, with 33.3 kN applied to each rod. While it is theoretically possible to apply a higher level of post-tensioning



(a) Dimensions of S0-FEA-Tshape



(b) Load-displacement diagram

Fig. 19. Deck's depth influence.

Table 5
Summary of the study’s results.

Specimen	f_c (MPa)	d_{deck} (mm)	d_{rod} (mm)	ρ_{rod} (%)	f_{pt} (MPa)	Further description	K_{el} (kN/mm)	$F_{13\text{ mm}}$ (kN)	$M_{13\text{ mm}}$ (kN.m)
S0-EXP	37	125	62.5	2.2	0	-	0.33	4.96	2.2
S21-EXP	37	125	62.5	2.2	48.4	-	1.26	11.5	4.8
S32-EXP	37	125	62.5	2.2	73.8	-	2.48	16.4	6.8
S43-EXP	37	125	62.5	2.2	99.1	-	2.93	19.8	8.3
S0-FEA	37	125	62.5	2.2	0	-	0.6	7.9	3.2
S43-FEA	37	125	62.5	2.2	99.1	-	2.63	17.6	7.3
S43-FEA-L0	37	125	62.5	2.2	99.1	Load on the joint (a/d_{rod} : 14.4)	1.14	11.3	5.4
S43-FEA-L750	37	125	62.5	2.2	99.1	Load 750 mm from the joint (a/d_{rod} : 2.4)	61.5	198	27.1
S0-FEA-Dil15	37	125	62.5	2.2	99.1	Dilation angle 15°	0.31	4.8	2.13
S0-FEA-Dil55	37	125	62.5	2.2	99.1	Dilation angle 55°	0.34	5.01	2.2
S43-FEA-50MPa	50	125	62.5	2.2	99.1	-	2.61	18.5	7.6
S43-FEA-75MPa	75	125	62.5	2.2	99.1	-	2.63	19.8	8.2
S70-FEA	37	125	62.5	2.2	161.5	-	3	29.2	12.1
S100-FEA	37	125	62.5	2.2	230.7	-	4.46	-	-
S0-FEA-SI	37	125	62.5	2.2	0	Single interlock	0.63	6.06	2.67
S0-FEA-MI	37	125	62.5	2.2	0	Multiple interlocks	0.33	-	-
S0-FEA-3rods	37	125	62.5	3.3	0	Adding a rod in the mid-section	0.32	5.98	2.65
S0-FEA-3rods-93	37	125	93.5	3.3	0	Effective depth: 102.5 mm	0.4	7.8	3.45
S0-FEA-SLM	37	125	93.5	3.3	0	Single layer with 62.5 mm depth	0.4	7.27	3.21
S0-FEA-SLT	37	125	93.5	3.3	0	Single layer with 30 mm depth	0.4	7.24	3.2
S0-FEA-SLTC	37	125	93.5	3.3	0	Single layer with 25 mm depth and additional rebar near the joint	0.4	7.2	3.18
S0-FEA-Tshape	37	250	175	1.84	0	-	0.58	10.5	4.63
S33-FEA-Mod	50	250	175	1.84	80	Modified design	2.96	35.6	15.69

numerically, practical constraints observed during the experimental program indicate that applying a post-tensioning force exceeding 35 kN on each rod using a wrench is challenging to achieve.

The initial bending stiffness of the S33-FEA-Mod closely matched that of the S43-EXP, with concrete initially crushing under an 8 kN load, which is attributed to the almost similar level of initial prestressing (Fig. 20). At this point, two concrete elements near the joint experienced compression, indicating a neutral depth of approximately 10–20 mm from the top fibre. After concrete crushing in the top flange, subsequent behaviour demonstrated nonlinear characteristics, with a steeper slope (nonlinear stiffness) than S43-EXP, leading to a 79 % higher load-carrying capacity within a serviceability range of 13 mm. This improvement is attributed to a higher gross moment of inertia and the arrangement of GFRP rods, with the tensioned rod at a greater depth contributing to increased load capacity. Placing a rod at a greater depth introduces a resistance moment ($A_f(f_f + f_{fe})e$) due to the eccentricity

from the centroid, as illustrated in (Fig. 19a). In the mentioned equation eccentricity is 100 mm the initial prestressing is 33 kN and the load level before joint opening varies from 0 to 5 kN (Fig. 5b), in the range of joint opening. Considering a cross-sectional area is homogeneous and the joint is still closed right after using the load (f_f is equal to zero), the elastic curve can be captured by (Eq. 4), where the first term accounts for the load applied, and the second term represents the effect of the resistance moment at the end anchorage.

$$\left(\frac{px}{1.789(EI)_{eq}} (1.9875 - x^2) \right) - \left(\frac{647x}{(EI)_{eq}} (5.78 - 5.1x + x^2) \right) \quad (4)$$

$$\left(\frac{px}{2.233\sqrt{f_c}} (1.9875 - x^2) \right) - \left(\frac{518x}{\sqrt{f_c}} (5.78 - 5.1x + x^2) \right) \quad (5)$$

The two top rods, having a negligible eccentricity of 5 mm, are close

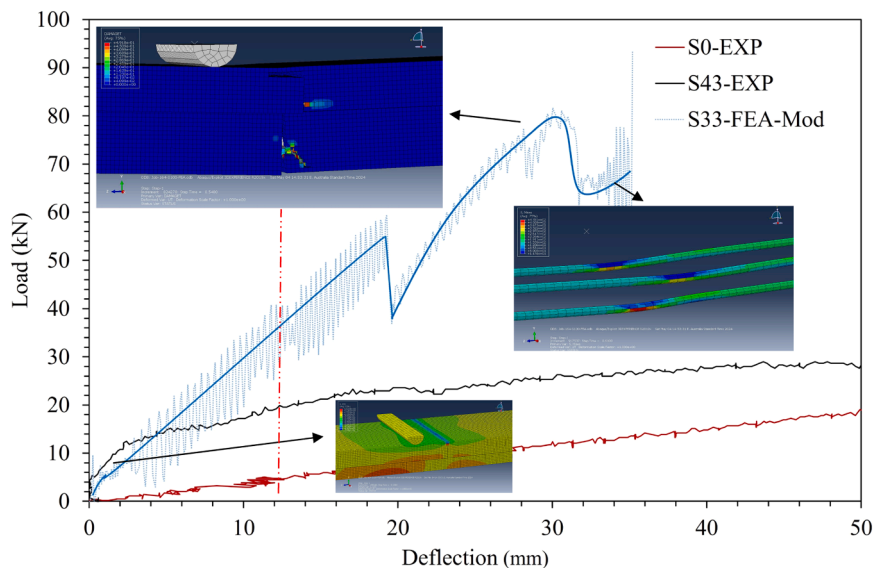


Fig. 20. Modified design.

enough to the centroid that their eccentricity can be disregarded in the calculation. By ignoring the presence of the GFRP rod and using an equation of ACI 318–08 [67] for concrete Modulus of elasticity, the equation can be rewritten in the form of (Eq. 5). However, as soon as the joint opens the curve of the segmental deck changes into a bilinear shape with a sharp turning point at the joint.

By continuing the loading, at an applied load of 60 kN and 28 mm deflection, the concrete surrounding the bottom rod in the web was crushed due to high compression stress from the GFRP rod. Additionally, at the ultimate stage, the internal rods experienced interlaminar shear on the upper surface. In contrast, the bottom rod endured 46 % higher tensile stress than the upper rods, owing to its greater depth. Accordingly, it can be mentioned the failure mechanism of the T-shape segmental post-tensioned concrete deck with an internal GFRP rod initiated the compression of the joint in the top part, followed by compression of the concrete around the rod with a higher depth and led to the interlaminar shear of the rods.

If the proposed segmental deck is intended to function as a pontoon deck, its length would need to vary according to the design criteria for floating walkways and pontoons DTMR-2015 [41], which depends on the specific project requirements. To test the feasibility of this design, a third segment was added to the S33-FEA-Mod, increasing the total length of the segmental deck by 50 %. A similar load was then applied close to the joint of this extended deck (Fig. 21). The results indicate that extending the segmental deck by adding a third segment reduced initial stiffness and load-carrying capacity within the serviceability range. Specifically, the initial stiffness decreased to 1.38 kN/mm, representing a 53 % reduction, and the load-carrying capacity in the serviceability range dropped to 11.2 kN, a 65 % reduction. This means a 50 % increase in the length led to a 53 % decrease in the flexural performance in the elastic range but as the concrete entered the non-linear stage the reduction increased to 65 %. Beyond the serviceability range, the failure mechanism was primarily governed by compression at the joint's top. Despite these changes, the behaviour beyond the serviceability range showed no evidence of concrete crushing around the rod or interlaminar shear, as indicated by the absence of a drop in load-carrying capacity. This suggests that increasing the number of segments shifts the behaviour from flexural-shear to flexural, resulting in lower stiffness due to a higher span-to-depth ratio. The results show that adding a segment to the system and increasing the length of the segmental deck by 50 % necessitates a 66 % increase in tension on each rod to maintain the same behaviour within the serviceability range. Beyond this range, adding

segments leads to increased concrete compression in the joint and reduced susceptibility to interlaminar shear. However, prestressing makes the failure concentrated between the joint and the loading point. Ultimately, the final failure is governed by the compressive crushing of concrete near the bottom rod.

6. Analytical evaluation

In monolithic reinforced concrete beams, the shear force is transmitted through the uncracked concrete in the compression zone, the interlocking action of aggregates across cracks, dowel action from longitudinal reinforcement, and arch action. In segmental concrete decks, particularly those reinforced with unbonded GFRP rods, the primary mechanisms shift to the uncrushed concrete and aggregate interlock within the compression zone of the joint, extending from the joint to the loading point. Increasing the initial prestressing causes a higher compression depth which provides a bigger compression zone in the joint. The unbonded internal GFRP rods provide the dowel action, as internal reinforcement does not contribute to shear resistance. Arch action is significant when the load is near the support and away from the joint, though its effect is negligible under critical loading near the joint. In addition to these, the shear failure mechanism of the monolithic beams is typically considered to be shear-compression or diagonal tension failure. However, the failure mechanism of the concrete segmental deck can be summarized in the compression of the joint and interlaminar shear failure of the GFRP rod. Given these distinctions, there is a need to reevaluate existing predictive equations to better estimate the shear strength of segmental GFRP-reinforced concrete decks.

The shear resistance of the hand-tight monolithic concrete beam can be evaluated from the equations provided in ACI 440.1 R-15 ($\frac{2}{5} \sqrt{f_c} b_w k d$) [50]; Using this equation for the segmental concrete deck, however, will result in an overestimation. The equation provided in ACI 440.4 R-04 ($0.17 \sqrt{f_c} b_w d$) [49], can be used for the monolithic prestressing members. It should be mentioned to all members that the stirrups were not utilised, and the shear resistance is primarily dependent on the shear resistance of the concrete, V_c . On the other hand, AASHTO-2003 [68] provided an equation for estimating the shear capacity of the joint in a prestressed concrete segmental bridge with an external steel tendon ($A_k \sqrt{f_c} (12 + 0.017 \sigma_n) + 0.6 A_{sm} \sigma_n$) [68]. This equation is in imperial units that must be translated into the SI unit. It is to be noted that the

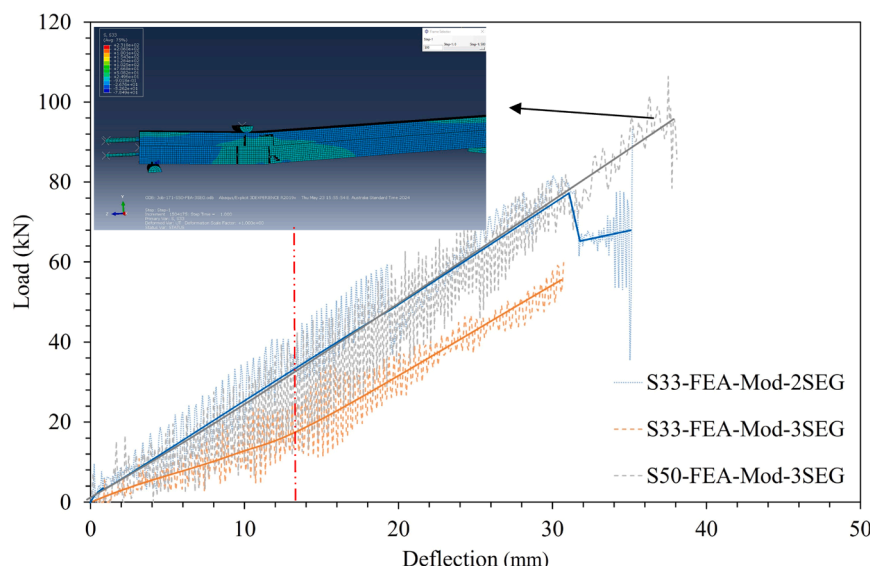


Fig. 21. Load-displacement in longer length.

experimental value is the maximum load-carrying capacity achieved during the test in which the concrete is crushed completely.

Among the codes used to predict the shear strength of the hand-tight specimen (S0-EXP), ACI 440.1 R-15 [50] proved the most accurate (with an error of 8.9 %). This accuracy is largely attributed to the inclusion of the ratio of the depth of the neutral axis to the reinforcement depth $(\sqrt{2\rho_f n_f + (\rho_f n_f)^2} - \rho_f n_f)$ [50] in the equation, effectively considering the impact of the GFRP rod reinforcement ratio, the concrete's compressive strength, and the modulus of elasticity of the GFRP rod by having $n_f \left(\frac{E_c}{E_f}\right)$. In contrast, ACI 440.4 R-04 [49] and AASHTO-2003 [68] tend to overestimate the shear strength of the segmental concrete deck for differing reasons. ACI 440.4 R-04 uses an equation designed for monolithic pre-stressed concrete sections with FRP tendons, which does not account for the joint-related reductions in load-bearing capacity caused by joint opening and stress concentrations. Moreover, ACI 440.4 R-04 [49] assumes the shear transfers through the concrete, therefore the effect of the prestressing (when the stirrups are not used) is not considered. However, the error is reduced with the increase in prestressing level, which shows that the behaviour of post-tensioned segmental decks is becoming similar to the monolithic section. Meanwhile, AASHTO-2003 [68] presupposes using external steel tendons for post-tensioning in segmental slabs and assumes the presence of a shear key between segments, which was not the case for segmental pontoon decks. By substituting the compression depth of the specimen (c) instead of the depth of the rod in the equation provided by ACI 440.4 R-04 [49], using (Eq. 6), the resulting strength (Table 6) closely matches the load corresponding to the opening of the joint, approximately 0.3 mm (Fig. 5c). This alignment suggests the initiation of concrete crush observed in the experimental setup. It needs to be mentioned in the proposed equation, that n is the number of rods (in this set of samples is equal to 2), and this might be limited to the segmental system with a rectangular cross-sectional area under the three-point loading and the influence of the environmental factors impose changes. Moreover, it has been assumed that rods located under tension and the possible presence of the pre-tensioned rods in compression have been ignored.

$$\frac{8}{17} k \left(\frac{n A_f (f_f + f_{fe})}{\sqrt{f_c} \beta_1} \right) \tag{6}$$

7. Conclusion

This study investigates the behaviour of post-tensioned segmental decks reinforced exclusively with non-corrosive GFRP rebar and rods. Finite element analysis was conducted alongside a parametric study to optimise the concrete pontoon deck design and manufacturing process and to provide design guidelines. Additionally, an analytical evaluation of the capacity of the segmental pontoon decks following code prediction equations was performed. The segmental deck has great potential for many maritime structures including pontoon decks and boating infrastructure as it is easy to assemble, non-corrosive, capable of

replacement, and easy to handle, making it a cost-effective solution for onshore marine infrastructures. The key findings from this work are the following:

- Post-tensioning the GFRP rod connecting the concrete segments significantly reduces self-weight deflection and increases initial stiffness and load-carrying capacity within the serviceability range because of the joint's low rotation and increase in the depth of concrete in compression.
- Post-tensioning leads to a more uniform stress distribution along the GFRP rod and reduces strain at the joint eliminating interlaminar shear failure. The discontinuity of the segments because of the joint causes an almost zero contribution of the internal GFRP reinforcement.
- The joint is the weakest part of the segmental pontoon deck system. Failure of the segments occurred in this location involving concrete crushing at the top, followed by interlaminar shear failure of the GFRP rod for systems with low levels of post-tension.
- A well-defined numerical model can accurately predict the post-tension segmental concrete deck behaviour, with the most significant performance factors being the level of post-tensioning, deck geometry, rod depth and number, while concrete compressive strength and dilation angle are less influential.
- Existing codes designed for segmental decks with steel tendons or monolithic prestressed members tend to overestimate the capacity of segmental concrete decks. A slight modification to the ACI 440.4 R-04 equation accounting for the compression depth of the joint instead of the rods' depth can provide a more accurate estimation of concrete crushing at the joint.

The joint cracking, and GFRP rod/concrete interaction at the joint governed the shear response of the segmental deck, hence, extra investigation, especially the fatigue behaviour and concrete cracking mechanism needs to be further explored.

CRediT authorship contribution statement

Shahrad Ebrahimzadeh: Writing – original draft, Validation, Software, Methodology, Formal analysis, Data curation, Conceptualization. **Senarath Weerakoon:** Writing – review & editing, Supervision, Resources, Project administration, Funding acquisition, Conceptualization. **Charles Dean Sorbello:** Writing – review & editing, Supervision, Resources, Project administration, Funding acquisition, Conceptualization. **Omar Saleh AlAjarmeh:** Writing – review & editing, Supervision, Resources, Methodology, Formal analysis, Conceptualization. **Allan Manalo:** Writing – review & editing, Supervision, Resources, Project administration, Investigation, Funding acquisition, Conceptualization. **Brahim Benmokrane:** Writing – review & editing, Supervision. **Reza Hassanli:** Writing – review & editing, Supervision.

Table 6
Theoretical evaluation.

Specimen	Guideline	Experiment (kN)	Predicted (kN)	Error (%)	Compression depth (mm)	Strength based on (ACI 440.4 R-04)
S0-EXP	ACI 440.1 R–15	26.7	24.3	8.9	8.92	5.5
	ACI 440.4 R–04		38.8	45.3		
	AASHTO 2003		32.26	20.8		
S21-EXP	ACI 440.4 R–04	27.6	38.8	40.5	11.33	7
	AASHTO 2003		41.6	50.7		
S32-EXP	ACI 440.4 R–04	30.68	38.8	26.4	12.23	7.6
	AASHTO 2003		45.3	47.6		
S43-EXP	ACI 440.4 R–04	31.1	38.8	24.7	13.14	8.2
	AASHTO 2003		49.3	58.5		

Declaration of Generative AI and AI-assisted technologies in the writing process

The authors would like to declare any AI-assisted technologies in the writing process are only used to improve readability.

Declaration of Competing Interest

The authors would like to declare and confirm that there is no conflict of interest of this manuscript.

Acknowledgement

The authors acknowledge the financial support from the Cooperative Research Centre Project (CRCPXIII000007) and the Maritime Safety Queensland of the Queensland Department of Transport and Main Roads.

References

- Al-Mosawe D, Neves L, Owen J. Reliability Analysis of Deteriorated Post-tensioned Concrete Bridges: The Case Study of Ynys-y-Gwas Bridge in UK (July). In *Structures*, 41. Elsevier; 2022. p. 242–59 (July).
- Wang X, Stewart MG, Nguyen M. Impact of climate change on corrosion and damage to concrete infrastructure in Australia. *Clim Change* 2012;110(3-4): 941–57.
- Ahmad S, Endo S. Australia country report. *Energy Outlook Energy Sav Potential East Asia 2020* 2021:33.
- Albidah A, Altheeb A, Alrshoudi F, Abadel A, Abbas H, Al-Salloum Y. Bond Performance of GFRP and Steel Rebars Embedded in Metakaolin Based Geopolymer Concrete (October). In *Structures*, 27. Elsevier; 2020. p. 1582–93 (October).
- Machello C, Bazli M, Rajabipour A, Hadigheh SA, Rad HM, Arashpour M, et al. FRP Bar and Concrete Bond Durability in Seawater: A Meta-analysis Review on Degradation Process, Effective Parameters, and Predictive Models (April). In *Structures*, 62. Elsevier; 2024, 106231 (April).
- Harle SM. Durability and Long-term Performance of Fiber Reinforced Polymer (FRP) Composites: A Review. In *Structures*, 60. Elsevier; 2024, February, 105881.
- Xin Q, Niu Q, Zhang M, Li Z, Gao R. Effect of Chlorine Salt Erosion on Flexural Performance of Gfrp and Steel Bars Hybrid Reinforced Beams. In *Structures*, 59. Elsevier; 2024, January, 105779.
- Chen Z, Huang Y, Zhou J, Dai S. Parametric Study, Finite Element Analysis, and Load Capacity Calculation for Flexural Behaviour of Seawater and Sea Sand Concrete Beams Reinforced With GFRP Bars. In *Structures*, 63. Elsevier; 2024, May, 106424.
- Tuwair H, Volz J, ElGawady M, Mohamed M, Chandrashekhara K, Birman V. Behavior of GFRP Bridge Deck Panels Infilled with Polyurethane Foam under Various Environmental Exposure. In *Structures*, 5. Elsevier; 2016, February. p. 141–51.
- Fasil M, Rahman MK, Al-Zahrani MM, Nanni A, Al-Osta MA, Al-Ghamdi SA, et al. Long-term field monitoring of slabs-on-ground reinforced with GFRP bars. *Constr Build Mater* 2023;404:133259.
- Wei J, Ke L, Wang P, Li W, Leung CK. Microstructure, mechanical properties and interaction mechanism of seawater sea-sand engineered cementitious composite (SS-ECC) with glass fiber reinforced polymer (GFRP) bar. *Compos Struct* 2024;343: 118302.
- Dong Z, Wu G, Xu B, Wang X, Taerwe L. Bond durability of BFRP bars embedded in concrete under seawater conditions and the long-term bond strength prediction. *Mater Des* 2016;92:552–62.
- Zhang P, Hu Y, Pang Y, Zhang S, Zia A, Gao D, et al. Experimental Study on the Bond Behavior of Gfrp Plate-high-strength Concrete Composite Interfaces under the Coupled Effects of Sustained Load and Seawater Immersion. In *Structures*, 30. Elsevier; 2021, April. p. 316–28.
- Sebaey TA. Crashworthiness of GFRP composite tubes after aggressive environmental aging in seawater and soil. *Compos Struct* 2022;284:115105.
- Micelli F, Nanni A. Durability of FRP rods for concrete structures. *Constr Build Mater* 2004;18(7):491–503.
- AlAjarmeh O, Manalo A, Benmokrane B, Schubel P, Zeng X, Ahmad A, et al. Compression behavior of GFRP bars under elevated In-Service temperatures. *Constr Build Mater* 2022;314:125675.
- Yang X, Alajarmeh O, Manalo A, Benmokrane B, Gharineiat Z, Ebrahimpzadeh S, et al. Torsional behavior of GFRP-reinforced concrete pontoon decks with and without an edge cutout. *Mar Struct* 2023;88:103345.
- Ebrahimpzadeh S, Yang X, Manalo A, Alajarmeh O, Senselova Z, Sorbello CD, et al. Flexural Behaviour of GFRP-Reinforced Concrete Pontoon Decks under Static Four-point and Uniform Loads. In *Structures*, 59. Elsevier; 2024, January, 105796.
- Elhamaymy A, Mohamed HM, Benmokrane B. Durability assessment and behavior under axial load of circular GFRP-RC piles conditioned in severe simulated marine environment. *Eng Struct* 2021;249:113376.
- Spagnuolo S, Giorgi C, Rinaldi Z, Pedrocchi L. Precast high-performance concrete (HPC) sheet piles prestressed with glass fiber reinforced polymer (GFRP) bars. *Compos Struct* 2023;304:116324.
- Benmokrane B, Mohamed H, Ahmed E. Recent developments of FRP bars as internal reinforcement in concrete structures & field applications. *Fourth Int Conf Sustain Constr Mater Technol Las Vegas NV 2016*, August.
- Rossini M, Benzecry V, Steputat C, Morales C, Nolan S, Nanni A. Marine Dock with FRP Bars and Seawater-Mixed Concrete. In *Italian Concrete Conference*. Cham: Springer Nature Switzerland; 2021, April. p. 17–29.
- Alagusundaramoorthy P, Reddy RVS. Testing and evaluation of GFRP composite deck panels. *Ocean Eng* 2008;35(3-4):287–93.
- Manalo A, Benmokrane B, Park KT, Lutze D. Recent developments on FRP bars as internal reinforcement in concrete structures. *Concr Aust* 2014;40(2):46–56.
- Zou Y, Yu K, Heng J, Zhang Z, Peng H, Wu C, et al. Feasibility study of new GFRP grid web-Concrete composite beam. *Compos Struct* 2023;305:116527.
- Manalo A, Alajarmeh O, Yang X, Ferdous W, Ebrahimpzadeh S, Benmokrane B, et al. Development and Mechanical Performance Evaluation of A GFRP-reinforced Concrete Boat-approach Slab. In *Structures*, 46. Elsevier; 2022, December. p. 73–87.
- El-Naqeeb MH, Ghanbari-Ghazijahani T, Gholampour A, Hassanli R, Zhuge Y, Ma X, et al. Cyclic Behaviour of an Innovative Cap Beam to Column Pocketless Connection in GFRP-RC Precast Structures (March). In *Structures*, 61. Elsevier; 2024, 106003 (March).
- Zhang Y, Li D. Seismic behavior and design of repairable precast RC beam-concrete-filled square steel tube column joints with energy-dissipating bolts. *J Build Eng* 2021;44:103419.
- Hu Z, Xu Z, Zhang S, Jiang H, Chen Y, Xiao J. Experimental study on shear behavior of precast high-strength concrete segmental beams with external tendons and dry joints. *Buildings* 2022;12(2):134.
- Le TD, Pham TM, Hao H. Numerical study on the flexural performance of precast segmental concrete beams with unbonded internal steel tendons. *Constr Build Mater* 2020;248:118362.
- Yuan A, He Y, Dai H, Cheng L. Experimental study of precast segmental bridge box girders with external unbonded and internal bonded posttensioning under monotonic vertical loading. *J Bridge Eng* 2015;20(4):04014075.
- Tran DT, Pham TM, Hao H, Chen W. Numerical investigation of flexural behaviours of precast segmental concrete beams internally post-tensioned with unbonded FRP tendons under monotonic loading. *Eng Struct* 2021;249:113341.
- Tran DT, Pham TM, Hao H, Chen W. Numerical study on bending response of precast segmental concrete beams externally prestressed with FRP tendons. *Eng Struct* 2021;241:112423.
- Le TD, Pham TM, Hao H, Yuan C. Performance of precast segmental concrete beams posttensioned with carbon fiber-reinforced polymer (CFRP) tendons. *Compos Struct* 2019;208:56–69.
- El-Naqeeb MH, Hassanli R, Zhuge Y, Ma X, Bazli M, Manalo A. Performance of GFRP-RC precast cap beam to column connections with epoxy-anchored reinforcement: a numerical study. *Arch Civ Mech Eng* 2024;24(2):1–26.
- El-Naqeeb MH, Hassanli R, Zhuge Y, Ma X, Manalo A. Numerical investigation on the behaviour of socket connections in GFRP-reinforced precast concrete. *Eng Struct* 2024;303:117489.
- Ghanbari-Ghazijahani T, Hassanli R, Manalo A, Smith ST, Vincent T, Gravina R, et al. Cyclic behavior of beam-column pocket connections in GFRP-reinforced precast concrete assemblies. *J Compos Constr* 2023;27(2):04022107.
- Baneshi V, Dehghan SM, Hassanli R. An experimental study on the in-plane behavior of interlocking blocks with different interconnection mechanisms. *Mater Struct* 2024;57(4):90.
- Ebrahimpzadeh S, Manalo A, Alajarmeh O, Yang X, Sorbello CD, Weerakoon S, et al. Flexural Behaviour of the Segmental Precast Concrete Decks Post-tensioned by GFRP Rods. In *Structures*, 65. Elsevier; 2024, July, 106712.
- DTMR. (2019). *Transport and Main Roads Specifications, MRTS72, Manufacture of Precast Concrete Elements*.
- DTMR. (2015). *Design Criteria for Floating Walkways and Pontoons*. Brisbane, Queensland: Queensland Department of Transport and Main Roads.
- Transport Roads & Maritime Services. (2015). *NSW Boat Ramp Facility Guidelines*. Available on website: (<https://www.transport.nsw.gov.au/system/files/media/documents/2023/nsw-boat-ramp-facility-guidelines.pdf>).
- DTMR. (2018). *Transport and Main Roads Specifications MRTS70 Concrete, Transport and Main Roads Specifications*.
- Standards Australia. (2018). *AS3600: 2018—Concrete Structures*.
- Australia S. *Methods of Testing Concrete-Compressive Strength Tests-Concrete, Mortar and Grout Specimens*. AS1012.9. Sydney. New South Wales, Australia: Standards Australia; 2014.
- Canadian Standards Association. (2019). *Specification for fibre-reinforced polymers (CAN/CSA S807-19)*. Rexdale, ON, Canada.
- ASTM D. Standard test method for tensile properties of fiber-reinforced polymer matrix composite bars. *ASTM 2011:D7205-11*.
- Alajarmeh O, Manalo A, Benmokrane B, Ferdous W, Mohammed A, Abousnina R, et al. Behavior of circular concrete columns reinforced with hollow composite sections and GFRP bars. *Mar Struct* 2020;72:102785.
- ACI. (2004). *ACI 440.4 R-04. Prestressing concrete structures with FRP tendons*.
- American Concrete Institute. *Guide for the Design and Construction of Structural Concrete Reinforced with Fiber-reinforced Polymer (FRP) Bars*. (ACI 440.1 R-15). Farmington Hills, Michigan: American Concrete Institute; 2015.
- Niwa J, Matsumoto K, Sato Y, Yamada M, Yamauchi T. Experimental study on shear behavior of the interface between old and new deck slabs. *Eng Struct* 2016; 126:278–91.

- [52] Systèmes, D. (2019). Abaqus/CAE user's manual. Dassault Systèmes Simulia Corp: Providence, RI, USA.
- [53] Carreira DJ, Chu KH. Stress-strain relationship for plain concrete in compression. *J Proc* 1985, November;82(6):797–804.
- [54] Mansour W. Numerical analysis of the shear behavior of FRP-strengthened continuous RC beams having web openings. *Eng Struct* 2021;227:111451.
- [55] Australian Standard, A. S. 4997, 2005. Guidelines for the Design of Maritime Structures.
- [56] Elchalakani M, Karrech A, Dong M, Ali MM, Yang B. Experiments and Finite Element Analysis of GFRP Reinforced Geopolymer Concrete Rectangular Columns Subjected to Concentric and Eccentric Axial Loading. In *Structures*, 14. Elsevier; 2018, June. p. 273–89.
- [57] Lee SH, Abolmaali A, Shin KJ, Lee HD. ABAQUS modeling for post-tensioned reinforced concrete beams. *J Build Eng* 2020;30:101273.
- [58] Othman H, Marzouk H. Applicability of damage plasticity constitutive model for ultra-high performance fibre-reinforced concrete under impact loads. *Int J Impact Eng* 2018;114:20–31.
- [59] Papanikolaou VK, Kappos AJ. Confinement-sensitive plasticity constitutive model for concrete in triaxial compression. *Int J Solids Struct* 2007;44(21):7021–48.
- [60] Wosatko A, Winnicki A, Polak MA, Pamin J. Role of dilatancy angle in plasticity-based models of concrete. *Arch Civ Mech Eng* 2019;19:1268–83.
- [61] Sümer Y, Aktaş M. Defining parameters for concrete damage plasticity model. *Chall J Struct Mech* 2015;1(3):149–55.
- [62] Chen L, Graybeal BA. Modeling structural performance of ultrahigh performance concrete I-girders. *J Bridge Eng* 2012;17(5):754–64.
- [63] Jabbar AM, Hamood MJ, Mohammed DH. Impact of Dilation Angle and Viscosity on the Ultra-High Performance Concrete Behavior in Abaqus. In 2021 International Conference on Advance of Sustainable Engineering and its Application (ICASEA). IEEE; 2021, October. p. 125–30.
- [64] Campione G, Monaco A, Minafo G. Shear strength of high-strength concrete beams: modeling and design recommendations. *Eng Struct* 2014;69:116–22.
- [65] Raza A, Ahmad A. Numerical investigation of load-carrying capacity of GFRP-reinforced rectangular concrete members using CDP model in ABAQUS. *Adv Civ Eng* 2019:2019.
- [66] Issa MA, Abdalla HA. Structural behavior of single key joints in precast concrete segmental bridges. *J Bridge Eng* 2007;12(3):315–24.
- [67] ACI Committee. Building code requirements for structural concrete (ACI 318-08) and commentary. American Concrete Institute; 2008.
- [68] AASHTO. (2003). Interim Revisions to the Guide Specifications for Design and Construction of Segmental Concrete Bridges.
- [69] Su Z, Zheng W, Wang Y, Hou X. Seismic vulnerability analysis of masonry structures built with disassembled brick wall sections. *Buildings* 2022;12(11):1831.
- [70] Nasrollahzadeh K, Ebrahimzadeh S. Numerical evaluation of unreinforced masonry brick walls retrofitted by polypropylene straps subjected to lateral loading. *AUT J Civ Eng* 2022;6(4):447–60.
- [71] Hu M, Jia Z, Han Q, Bai Y, Jiao C, Long P. Application of CFRP tendons to novel connections of precast concrete deck panels: experiments and analytical models. *J Compos Constr* 2023;27(1):04022085.
- [72] Le TD, Pham TM, Hao H, Li H. Behavior of precast segmental concrete beams prestressed with external steel and CFRP tendons. *J Compos Constr* 2020;24(5):04020053.